Plasma Source Development for Fusion-Relevant Material Testing

J.B.O. Caughman[a)], R.H. Goulding, T.M. Biewer, T.S. Bigelow, I.H. Campbell, J. Caneses, S.J. Diem, A. Fadnek, D.T. Fehling, R.C. Isler, E.H. Martin, C.M. Parish, J. Rapp, and K. Wang
Oak Ridge National Laboratory, Oak Ridge, TN 37831, USA

C.J. Beers, D. Donovan, N. Kafle, H. B. Ray, G.C. Shaw, M.A. Showers
University of Tennessee, Bredesen Center, Knoxville, TN 37996, USA

[a)]Electronic mail: caughmanjb@ornl.gov

Plasma-facing materials in the divertor of a magnetic fusion reactor have to tolerate steady-state plasma heat fluxes in the range of 10 MW/m^2 for ~10^7 s, in addition to fusion neutron fluences, which can damage the plasma-facing materials to high displacements per atom (dpa) of ~50 dpa. Materials solutions needed for the plasma-facing components are yet to be developed and tested. The Materials Plasma Exposure eXperiment (MPEX) is a newly proposed steady-state linear plasma device designed to deliver the necessary plasma heat flux to a target for testing, including the capability to expose a priori neutron-damaged material samples to those plasmas. The requirements of the plasma source needed to deliver the required heat flux are being developed on a Proto-MPEX device, which is a linear high-intensity radio-frequency (RF) plasma source that combines a high-density helicon plasma generator with electron- and ion-heating sections. The device is being used to study the physics of heating overdense plasmas in a linear configuration. The helicon plasma is operated at 13.56 MHz with RF power levels up to 120 kW. Microwaves at 28 GHz (~30 kW) are coupled to the electrons in the overdense helicon plasma via electron Bernstein waves, and ion cyclotron heating at 7–9 MHz (~30 kW) is

via a magnetic beach approach. High plasma densities > $6 \times 10^{19}/m^3$ have been produced in deuterium, with electron temperatures that can range from 2 to > 10 eV. Operation with on-axis magnetic field strengths between 0.6 and 1.4 T is typical. The plasma heat flux delivered to a target can be > 10 MW/m^2, depending on the operating conditions. An initial plasma material interaction experiment with a thin tungsten target exposed to this high heat flux in a predominantly helium plasma showed helium bubble formation near the surface, with no indication of source impurity contamination on the target.

I. INTRODUCTION

The availability of a fusion reactor is determined to a large extent on the lifetime of its plasma-facing components. Developing materials resistant to high erosion and neutron radiation damage is a grand challenge that urgently needs to be addressed.[1] The materials used in a fusion device must withstand an intense plasma heat flux. The divertor in a tokamak is exposed to plasma heat fluxes of ~10 MW/m^2 and transient high-energy fluxes of 0.5 MJ/m^2 from edge-localized modes (ELMs).[1,2] The development of divertor materials, including neutron irradiation–resistant materials, for reactor conditions is an active research area.[3] It is recognized that new testing capabilities, especially new plasma-material interaction (PMI) facilities, are needed for development of new plasma-facing materials and components; [1,4] and new facilities are under construction worldwide.[5,6] Oak Ridge National Laboratory proposes a new Material Plasma Exposure eXperiment (MPEX) [7,8], which will use a new high-intensity plasma source concept. The source is electrodeless so that impurity generation in the source region, which could harm the interpretation of PMI processes, will be minimized.

Requirements for the new MPEX include a target electron density of 10^{20} to $10^{21}/m^3$, electron temperature of 1–15 eV, ion temperatures of up to 25 eV, a plasma heat flux of >10 MW/m^2, and a target magnetic field of 1–2 Tesla. These parameters will allow for material testing in tokamak divertor relevant plasmas.[1] The MPEX design uses a helicon plasma source with the ability to heat electrons and ions via electron Bernstein waves (EBWs) and ion cyclotron heating (ICH), respectively. The resulting plasma will allow for PMI experiments at fusion-relevant conditions, including the ability to test neutron-irradiated samples.

The plasma source needed for MPEX is being developed on a Proto-MPEX device, which is described subsequently. One of the primary goals of this experiment is the demonstration of the power coupling physics needed to deliver the desired plasma heat flux at a target (~10 MW/cm^2). Proto-MPEX combines a helicon plasma source with an electron heating section using 28 GHz microwaves and an ion heating section with RF power at 7-9 MHz. Details of the hardware and diagnostics are explained, as well as initial operating results for all the sources. Another goal of Proto-MPEX is to perform high-flux/low-fluence material tests at fusion-relevant conditions in deuterium, helium, or mixed helium/deuterium plasmas. Exploring helium plasma or mixed deuterium/helium plasmas can provide important information for the operational phases of ITER. ITER will most likely have a non-active phase of operation with helium to explore H-modes using the lower L-H power threshold of helium plasmas. During the active phase of ITER operation (or any fusion reactor), helium (the fusion ash) will be implanted in the divertor in small concentrations. Therefore, an initial PMI experiment in

a mostly helium plasma has been performed, and findings from this study are also included.

II. EXPERIMENTAL APPARATUS

A cross section of the Proto-MPEX is shown in Fig. 1. The device consists of a vacuum chamber with 12 solenoid magnets (M1 through M12), a helicon plasma source, a microwave coupling section, an ICH antenna, and "downstream" and "upstream" target plates. Throughout this paper, upstream refers to the area to the left of the helicon antenna and downstream refers to the area to the right of the antenna. Axial locations are often referenced with respect to the center of the helicon antenna.

The magnets have an inner diameter of 21.7 cm and are made of 40 turns of water-cooled copper conductor. They were originally constructed for the Elmo Bumpy Torus experiment [9] and are designed to operate continuously at 9,000 A. For our experiments, most of the coils typically operate at up to 6,500 A, which produces a peak magnetic field of approximately 1.5 T. The two magnets around the helicon antenna operate at currents of between 200 and 400 A, with magnetic fields up to ~0.1 T.

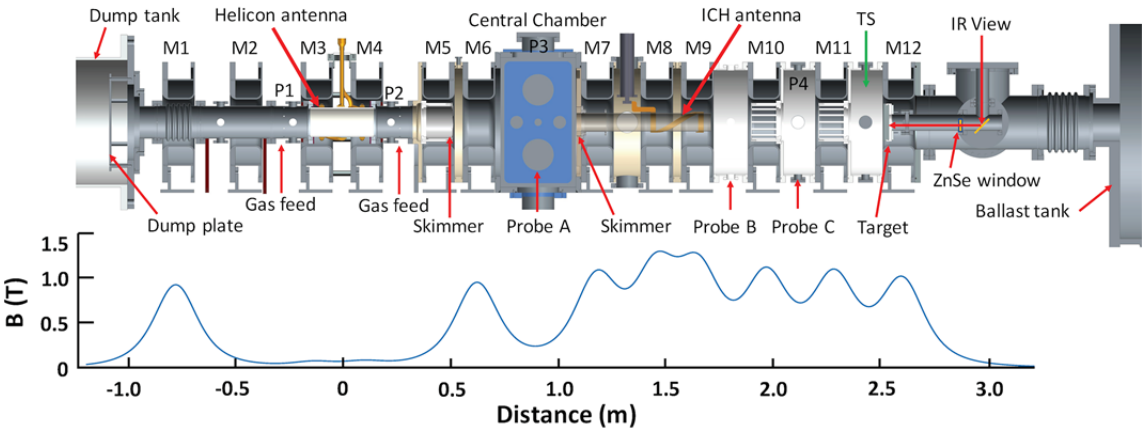

FIG. 1 (Color Online) Cross section of the Proto-MPEX device and a typical axial magnetic field strength. The coils are labeled a M1, M2, etc. For this field calculation, there is no current in coils M2 and M5. Coils M3 and M4 have 310 amperes, and the remaining coils have 5900 amperes. The central chamber is between coils M6 and M7 and is the location of Probe A, pressure measurement P3, and the microwave launchers. The direction of the magnetic field is from left to right in the figure.

The vacuum chamber and pumping system are composed of a variety of components. Starting on the left-hand side of Fig. 1, a large dump tank is located upstream of the helicon antenna and consists of a 66 cm long, 61 cm diameter stainless steel tank. A small 150 L/s turbo pump is located there as well. The section between the dump tank and the fifth magnet, M5, consists of standard 15.2 cm diameter stainless steel vacuum components. Downstream from that point, the vacuum chamber is formed by the aluminum housing of the magnets and stainless steel spool pieces (~49 cm inner diameter) that connect them. The "central chamber" shown in the figure is an aluminum box, 41 cm wide, 66 cm high, and 69 cm deep. A 2,800 L/s and a 1,000 L/s turbo pump are located there. A skimmer plate with a 5.8 cm diameter hole is located between the helicon antenna region and the central chamber to provide differential pumping. An additional skimmer plate with an 8.6 cm diameter hole is located on downstream of the central chamber. Beyond the target plate is a large-volume ballast tank (6.3 m^3) that provides effective pumping for pulsed gas operations and includes a 2,500 L/s turbo pump. The base pressure is ~10^{-6} Torr. There are two primary gas injection points, which consist of a gas ring wrapped around the circumference of the vacuum chamber. One injection point is located 14 cm upstream of the helicon window, and the other is 14 cm downstream of the window. Gas flows of up to 10 standard liters per minute (SLM) are

possible with flow controllers from MKS Instruments, though typical values are between 0.1 and 2.5 SLM.

MKS Instruments model 627 baratrons are used to measure the pressure at four locations (shown in Fig. 1 as P1-P4): 12 cm upstream of the helicon window, 12 cm downstream of the helicon window, in the central chamber, and at various locations between the central chamber and the target. The baratron heads are wrapped with several layers of mu metal and are mounted between 30 and 60 cm from the chamber walls to help mitigate effects of the magnetic field. Pulses of gas only, magnetic field only, and gas plus magnetic field are taken to calibrate out the effects of the field on the measurement. The gas pressure is highest near the helicon and lowest near the target for constant flow conditions without a plasma, when the gas is injected near the helicon. For example, a constant flow of 0.4 SLM results in a pressure of 10.5 mTorr near the antenna, 5.1 mTorr in the central chamber (0.94 m downstream of helicon), and 1.1 mTorr at 2.17 m downstream of the helicon. The gas pressure typically drops during the plasma pulse, presumably due to plasma pumping effects.

The helicon plasma source uses a water-cooled double-helix half-turn antenna, as shown in Fig. 2. The antenna is 25 cm long with an inner diameter of 15 cm. The antenna is separated from the vacuum chamber by a cylindrical aluminum nitride window (Ceradyne Ceralloy® 1370 DP) 30 cm long with an inner diameter of 13.8 cm. The antenna is operated at 13.56 MHz at power levels of up to 120 kW using a Continental Electronics model FRT-86 transmitter.

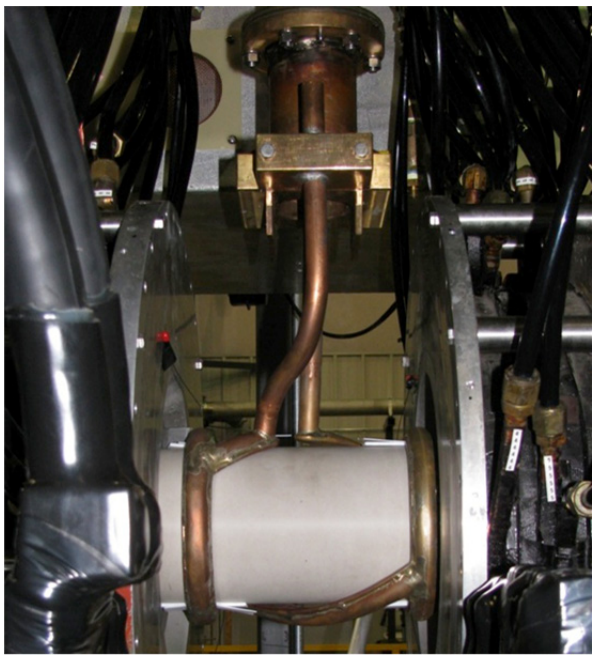

FIG. 2 (Color Online) Water-cooled helicon antenna and aluminum nitride ceramic tube.

Two different microwave systems are used to create and heat the plasma. An 18 GHz klystron source (Varian model VGA-934) is used to initiate the plasma. A short run of rectangular waveguide (~1.5 m of WR62), followed by a rectangular-to-circular convertor and a smooth-walled, up-taper section, direct the microwaves into the central chamber (see Fig. 1) through a 63 mm diameter, 2.8 mm thick aluminum oxide vacuum window. An internal reflector plate directs the microwaves toward the target side of the central chamber wall, where they are reflected again in the direction of the helicon source. Power levels of 4 to 8 kW are typically used to create a seed plasma before initiation of the helicon plasma.

Microwaves at 28 GHz are used to heat the plasma electrons, primarily via mode-converted EBWs. The EBW heating approach was chosen because the plasma density in the Proto-MPEX device is much higher than the cutoff density at 28 GHz (~$1 \times 10^{19}/m^3$). EBWs are hot electrostatic plasma waves that propagate in the plasma, do not have a

density cutoff, and are readily absorbed on Doppler-broadened electron cyclotron harmonic zones.[10] The TE02 output mode of the gyrotron (Varian model VGA-8000, 200 kW) is converted to the HE11 mode via a mode converter tank. A Vlasov launcher directs the microwaves toward a paraboloid reflector, which directs and focuses the resulting HE11 mode to the input of a 88.9 mm diameter section of corrugated waveguide (with 1.3 mm deep grooves spaced every 1.4 mm). The waveguide run to the experiment consists of 3.2 m of waveguide and two miter bends. The connection to the central chamber is through a corrugated taper to interface with a 63.5 mm diameter edge water-cooled aluminum oxide vacuum window. An additional section of 63.5 mm diameter corrugated waveguide (1 mm grooves spaced every 1.4 mm) and miter bend with waveguide extension, shown in Fig. 3, is used to direct the microwaves once inside the vacuum chamber. The miter bend/waveguide extension section can be rotated to find the optimum launch angle for EBW coupling. Most experiments have been with the launcher pointing in a direction of +20° from normal (as shown in the figure). Predictions of wave propagation and absorption have been made using the GENRAY-C code, which is a modification of the GENRAY code [11] that operates in Cartesian coordinates.

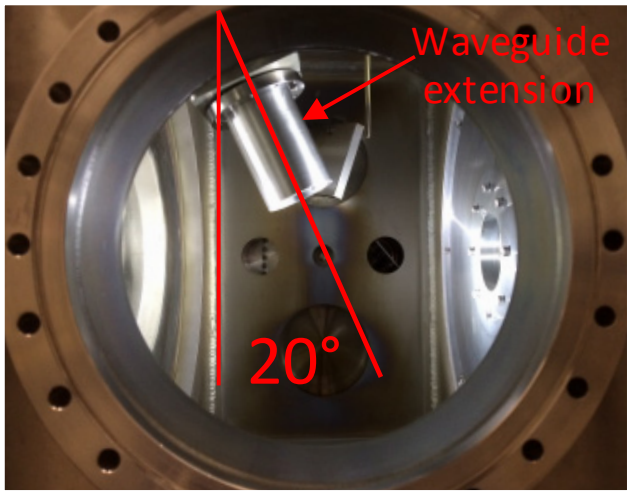

FIG. 3 (Color Online) Waveguide extension section inside the central chamber for EBW coupling showing a +20° launch angle with respect to normal. The direction of the magnetic field is from left to right in the figure. The 8.6 cm diameter skimmer can be seen on the right.

The ICH antenna section is located between the central chamber and the target. The antenna is a 25 cm long double-helix half-turn antenna with an inner diameter of 9 cm, similar in design to the helicon antenna but with the helical twist in the opposite direction. The installed antenna is shown in Fig. 4. The antenna is operated in-vacuum but is separated from the plasma by a 85 mm outer diameter, 80 mm inner diameter, 61 cm long quartz tube. The antenna is designed to couple energy to the ions via the slow wave magnetic beach approach [12–14], where the waves are absorbed at the cyclotron resonance in the expanding magnetic field just downstream of the antenna. The antenna has been modeled using the ANTENA code [15] to estimate loading and wave propagation and by CST Microwave Studio® to verify power handling capability. It is typically operated at 8.5 MHz and at up to 30 kW using a Continental Electronics model FRT-85 transmitter.

FIG. 4 (Color Online) ICH antenna on the Proto-MPEX before insertion of the quartz tube.

The plasma is terminated at both ends on conducting metal plates. The upstream plate located in the dump tank is 1.5 mm thick stainless steel with a diameter of 40 cm. The plate is large enough to capture the expanding magnetic field lines from the plasma. The target plate consists of either a 1.5 mm or a 0.25 mm thick stainless steel plate with a diameter of between 9.5 and 11.4 cm, depending on its location. For most experiments, the target is located 2.57 m downstream of the helicon antenna, but it was located 1.5 m downstream for some experiments. As discussed subsequently, an infrared (IR) camera was used to image the backside of the target plate to obtain an estimate of the deposited heat flux.

III. DIAGNOSTICS

Many different diagnostics are used at several axial and radial locations, including double Langmuir probes, Filterscopes, IR and fast digital cameras, a microwave interferometer, a retarding field energy analyzer, and a Thomson scattering system, some of which are described as follows.

Several double Langmuir probes are used to make radial profile measurements at various axial locations. The probes consist of two tungsten wires that are 0.25 mm in diameter, 1.2 mm long, and separated by 1.4 mm. The calculated density is within ~10% of the density determined using a 70 GHz interferometer. The sweep voltage was typically a triangle wave swept at +/- 70 volts at a frequency of 200 Hz. Data are shown at three different probe locations, as indicated in Fig. 1. Probe A is located in the central chamber and is 0.94 m downstream of the helicon antenna. Probes B and C are located 1.85 m and 2.17 m downstream of the antenna, respectively.

Filterscopes [16] are used at several axial locations to measure line emission from the plasma at a 100 kHz sample rate. Narrowband D-alpha filters (656 nm, 1 nm wide) are used most often, but various helium, tungsten, and other line filters have also been used [17]. The emission from the plasma is measured with compact achromatic collimating lenses and is connected to the Filterscope inputs via fiber-optic cable. Up to 24 simultaneous Filterscope measurements are possible. Fiber optic views are located between most of the magnets. When coupled with the fast sampling rate, the temporal and axial variation of the plasma emission can be measured. Applications include validation of B2-Eirene transport code predictions [18], understanding the temporal

evolution of the plasma during helicon plasma mode jumps, exploring recombination physics at the target from D-alpha, beta, gamma emission, and helium line ratio measurements to determine density and temperature [17].

A McPherson 2051 high-resolution spectrometer is available for use on the Proto-MPEX device. The spectrometer is a 1 m Czerny-Turner configuration with gratings ruled at 1800, 1200, and 300 groves/mm. A Princeton Instruments PhotonMAX 512b EMCCD camera is used as a detector. The system is used to measure the Doppler-broadened spectra of plasma impurity ions (typically Ar II from injecting ~1% argon in a deuterium plasma) with a 10 ms framing rate on 5 simultaneous lines of sight, using the same collection optics as are available for Filterscope measurements. For example,

A Thomson scattering system is used to measure the density and temperature in front of the target plate. It uses a Spectra Physics Quanta Ray Pro-350 Q-switch Nd:YAG laser. The laser is frequency doubled to produce 532 nm light at 10 Hz pulses. A Kaiser Optical Systems Holospec f/1.8 spectrometer with a PI-Max3 intensified CCD camera is used to measure the Thomson scattering signal. Details of the system can be found in Ref. 19.

The heat deposition profile at the target plate is measured by viewing the backside of the target with a FLIR A655sc IR camera. The target image is seen through a 4.6 cm diameter ZnSe window and is reflected from a gold-coated mirror to the camera. A fiducial pattern on the backside of the target is used to help focus the camera. An example view of the backside of the target is shown in Fig. 5. Details of the IR imaging system can be found in Ref. 20. For thicker target plates (1.5 mm), the temperature was measured with a thermocouple inserted into the edge of the plate. For the thinner plates

(0.25 mm), a thermocouple was attached 2.5 cm from the center of the plate. The plates were either bead-blasted or water-jetted to produce a dull surface finish. The target emissivity was estimated based on the thermocouple measurement and was calibrated with a heat gun during benchtop testing, with typical values of 0.33 for the thick plate and 0.26 for the thin plate. The target plates were supported and kept rigid with four 1.25 cm diameter aluminum rods attached to the edges of the plate, as can be seen in the figure. Note that the camera optics are such that the heat pattern seen in Fig. 7 corresponds to what would be observed when viewing the target from the helicon antenna.

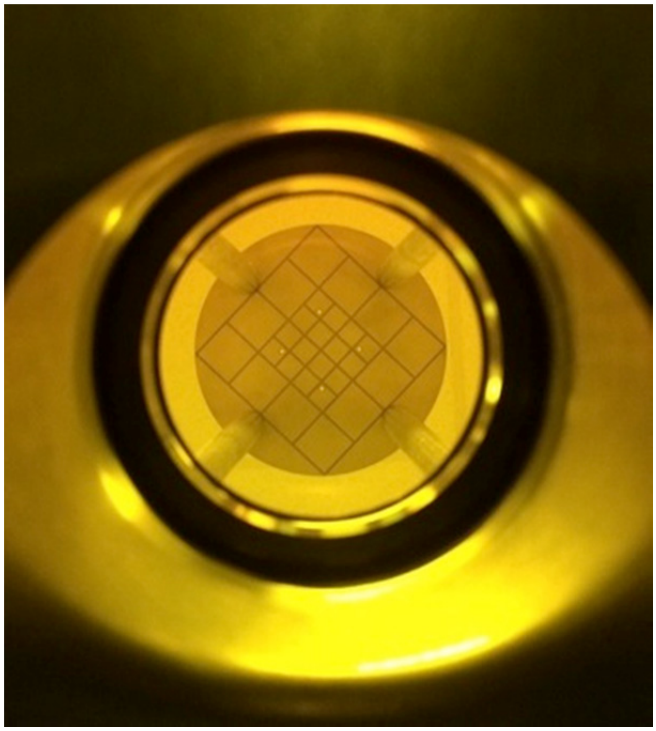

FIG. 5 Backside view of the 11.4 cm diameter target plate showing an example of a fiducial pattern. Smaller fiducial patterns were used for the target patterns shown in Fig. 7. Four 1.25 cm diameter aluminum rods around the edge support the targets and keep them rigid.

IV. INITIAL EXPERIMENT RESULTS AND DISCUSSION

The Proto-MPEX device has been operated with several different gases—including hydrogen, deuterium, helium, and argon—though most efforts focus on deuterium plasmas because of its high relevance for fusion plasma material interactions. The plasma is pulsed, with the 18 GHz system coming on first for pre-ionization followed by a pulse from the helicon source. The helicon pulse length is typically ~150 ms, but 1 second pulses have been obtained. The pulse length is primarily restricted by the lack of water cooling on the helicon vacuum window, although a new water-cooled window is being designed that will allow for much longer pulse operation. Microwaves at 28 GHz (30–60 ms pulse) and ICH power (30-60 ms pulse) near 8.5 MHz are initiated in the middle of the helicon pulse. A typical pulse, showing the timing of all the power system triggering, is shown in Fig. 6.

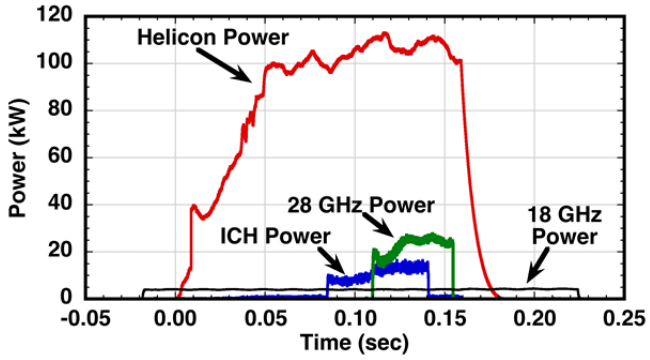

FIG. 6 (Color Online) A typical plasma pulse, showing the timing of the RF and microwave systems. The 18 GHz pulse (~4 kW) starts 20 ms before the helicon pulse (~110 kW), which is referenced at t=0. The 28 GHz pulse (~25 kW) and the ICH pulse (~14 kW) are in the middle of the helicon pulse.

The plasma parameters can vary depending on the magnetic field configuration, helicon power, gas pressure, and additional auxiliary heating power (e.g., EBW or ICH). Two primary helicon operating modes have been observed, with one being dominated by power coupling in the edge of the plasma and the other showing evidence for power coupling to the core of the plasma. The edge-coupled mode seems to be supported by a Trivelpiece-Gould (TG) mode [21]. Plasma density measured 1.5 m downstream of the helicon can vary from 1–2 × $10^{19}/m^3$ in the center of the plasma, with an electron temperature that can vary from a 2–4 eV in the center to > 7 eV in the edge (radius > 2 cm). An example of the heat deposition pattern (shown as the change in the temperature) on the thin target plate (0.25 mm) located 2.5 m downstream of the helicon antenna is shown in Fig. 7a, where two thin regions of high temperature are typically seen in the edges. Near-field capacitive coupling or inductive coupling could also be a contributing factor to this edge heating pattern. Similar edge heating patterns have been seen in visible light images in Ref. 22, as the plasma starts in E-mode before it transitions to H-mode. In general, the electron temperature increases and density decreases as the operating pressure decreases (e.g., from 10 mTorr to 2 mTorr in the central chamber). The density and electron temperature decrease as a function of distance from the source, with the density dropping 10–20% from 1.5 to 2.1 m away and the electron temperature dropping 40–50%. When combined with a focusing magnetic field to make a smaller diameter plasma (lower magnetic field in the helicon antenna region) and low gas flow (< 0.1 SLM, fill pressure < 2 mTorr), the peak plasma heat flux deposition on a target

located 1.5 m downstream from the antenna can be concentrated and exceed 10 MW/m^2 in a small area on target, based on IR camera measurements of the temperature change of the target (>300°C). For this condition, the electron temperature in the high heat flux region can be >20 eV. An example of the target heat flux pattern for this configuration is shown in Fig. 7b for the thick target plate (1.5 mm).

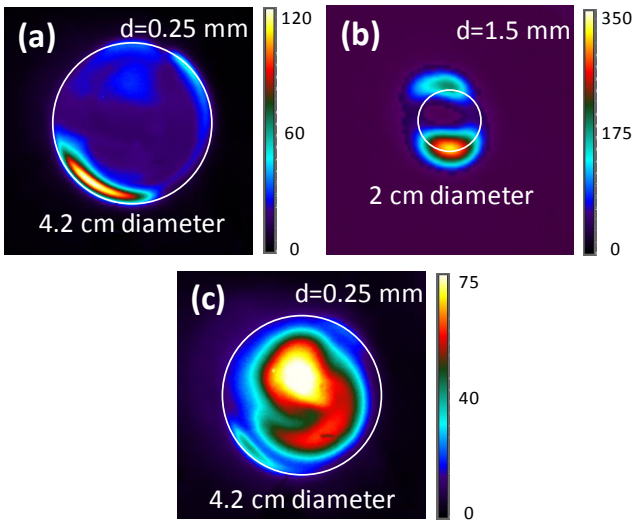

FIG. 7 (Color Online) Example of heat deposition profiles on the target plate. The change in the target temperature is shown (delta-T). A typical edge mode pattern (a) for a thin (d=0.25 mm) target plate. A focused-field edge mode pattern (b) for a thick (d=1.5 mm) target plate. A typical helicon-mode pattern (c) for a thin (d=0.25 mm) target plate. Units are in degrees Celsius.

When the helicon RF power exceeds a threshold level, typically >105 kW, the plasma experiences a mode jump that increases the core plasma density by more than a factor of 2. These center-coupled plasmas are much more quiescent compared with the edge-coupled mode plasmas. Electron densities greater than 7×10^{19}/m^3 have been measured with a double Langmuir probe located 2.1 m downstream of the helicon source,

which is 0.4 m from the target, while the electron temperature for this mode is 1.5–2 eV at this location. There values are consistent with the requirements of the helicon source for MPEX [18]. The probe results are consistent with Thomson scattering results of $7.6 \times 10^{19}/m^3$ and 1.5 eV measured 0.1 m in front of the target. An example of the heat deposition on the thin target plate (0.25 mm) for this mode is shown in Fig. 7c, where core power deposition is seen. The temporal behavior of this mode jump is shown in Fig. 8. For this condition, deuterium gas is injected 14 cm downstream of the helicon antenna at a flow rate of 2.4 SLM at 300 ms before the helicon power pulse and is then reduced to a rate of 1.7 SLM at 50 ms before application of 110 kW of helicon power. For this shot, the peak magnetic field was 1.3 Tesla, the magnetic field around the helicon antenna was 0.05 Tesla, the 18 GHz microwave power was 3 kW, and the central chamber pressure was ~2 mTorr during the plasma pulse. The timing of the mode jump is influenced by input power level, gas flow level/timing, and gas fueling location. Increased pumping in the central chamber and the use of smaller diameter skimmers could increase the downstream electron temperature and are being explored. Details of the helicon mode jump physics are described in Ref. 23.

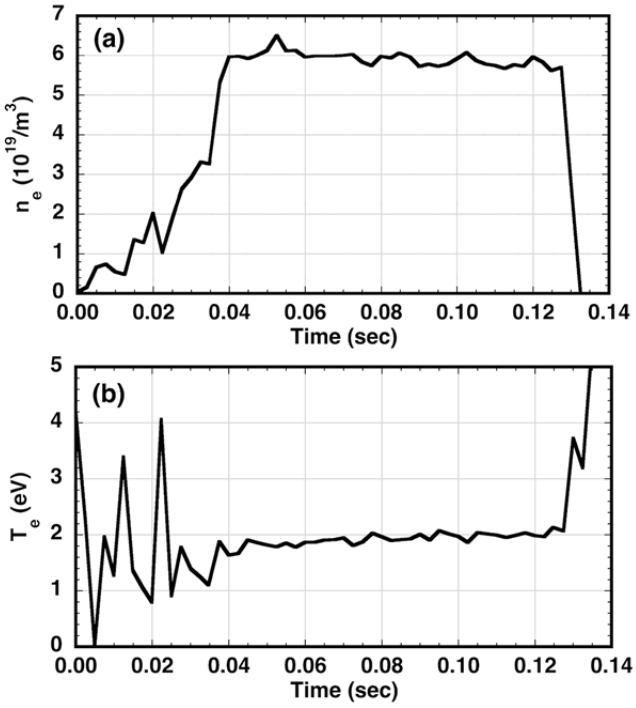

FIG. 8. Plasma density (a) and temperature (b) vs. time showing the transition to a high-density mode near 35 ms, measured on-axis 1.85 m downstream of the helicon antenna. The helicon power was 110 kW, the 18 GHz power was 3 kW, the peak magnetic was 1.3 Tesla, and the magnetic field at the helicon antenna was 0.05 Tesla. The central chamber pressure was ~2 mTorr.

Typical density and temperature profiles are shown in Fig. 9 for several axial locations. Probes A and B were scanned vertically, and Probe C was scanned horizontally. The experimental conditions were the same as for Fig. 8. The density is broader for Probe A because of the flux tube expansion in the central chamber. The central density does not vary much on axis, but the electron temperature tends to decrease further downstream. This temperature decrease might be caused by collisions with neutrals. The temperature profiles tend to be fairly flat in the center and peaked at the edges (>2 cm). The density is not radially symmetric, which is consistent with the heat deposition pattern

shown in Fig. 7c. Increasing the magnetic field in the helicon antenna region leads to larger diameter plasmas at the target, but more RF power will likely be needed to maintain the core-coupled mode and will be the subject of future experiments.

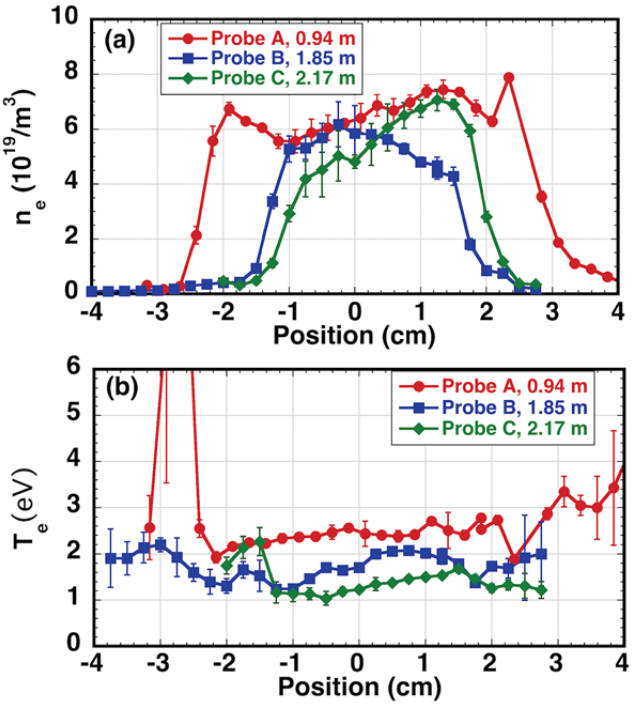

FIG. 9 (Color Online) Plasma density (a) and temperature (b) vs. radial position at several axial locations for the same experimental conditions shown in Fig. 8.

Microwave power at 28 GHz has been coupled to the plasma during overdense conditions. Most experiments have used the O-X-B mode conversion scenario, where an Ordinary-mode is launched from the waveguide at a tangential angle with respect to the magnetic field. The O-mode converts to the slow eXtraordinary mode near the upper hybrid resonance, where it then converts to the Bernstein wave. The Bernstein wave then propagates perpendicular to the magnetic field, where it is damped on the Doppler-broadened electron cyclotron harmonic surfaces.

A plot of the electron temperature and density as a function of time during a 28 GHz microwave pulse is shown in Fig. 10. These data were measured 1.85 m downstream of the helicon antenna (0.9 m downstream of the microwave launcher) in a deuterium discharge at a radius of 2 cm, with a launch angle of +20° from normal (as shown in Fig. 3) and a coil current of 4700 A. The peak magnetic field was 1.0 Tesla, the helicon antenna field 0.05 Tesla, and the field in the central chamber was ~0.3 Tesla. The helicon power was ~110 kW, the 18 GHz power was 3 kW, and the central chamber pressure during the plasma pulse was ~2 mTorr. A modest increase in the electron temperature was observed (~25%) at this radial location during the microwave pulse, where the electron temperature increases from ~3 to ~3.8 eV. GENRAY-C modeling predicts that the power absorption should be near the upper hybrid layer at the plasma edge (radius of ~3 cm in the central chamber) but with areas of better core coupling existing at certain values of the magnetic field where Doppler-broadened resonances are accessible [24]. The modeling suggests that the edge coupling will be dominant as a result of collisional damping, which is consistent with experimental observations of power deposition in the edge; however, the situation should improve at lower neutral density and higher electron temperature. Recently it has been observed that longer plasma pulse lengths result in lower neutral pressure (<1 mTorr during the plasma pulse) near the EBW launcher because of plasma pumping in the central chamber. This pressure reduction and the use of improved (smaller diameter) skimmer plates for better differential pumping are being explored as a way to improve EBW core coupling, along with increasing the power level and pulse length of the microwave system.

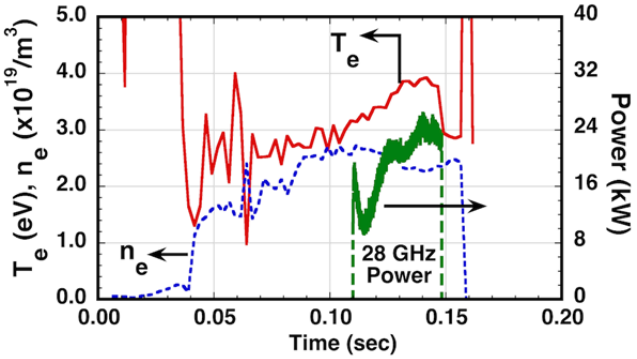

FIG. 10 (Color Online) Change in electron temperature and density as a function of time resulting from the injection of ~20 kW of microwave power at 28 GHz into a deuterium plasma with 110 kW of helicon power, 3 kW of 18 GHz power, and a central chamber pressure of ~2 mTorr. Data were measured 1.85 m from the helicon antenna (0.9 m from the EBW injection location) at a radius of 2 cm, with an EBW launch angle of +20°.

The ICH antenna has been operated at 8.5 MHz and at up to 25 kW for 60 ms pulses into a helicon plasma with deuterium plasma densities of 2–6 × 10^{19}/m^3 and coil currents of 5900 and 6400 A. These conditions correspond to a drive-frequency-to-ion-cyclotron-frequency ratio (ω/ω_{ci}) of 0.85 and 0.79, respectively. Operations thus far have focused on measuring the antenna loading to determine power-handling limits, but some initial heating experiments have also been performed. The predicted loading of the antenna (real part of the antenna load impedance) by the ANTENA code is shown in Fig. 11 as a function of plasma density and the gap between the antenna and the plasma edge. The measured load impedance of 4–5 ohms is somewhat higher than predicted for the measured gap of 2 to 2.5 cm. Contributing factors for this difference include the one-dimensional assumptions in ANTENA, the actual radial density profile, and the changing magnetic field. We are in the processing of modeling the antenna in 3-D using COMSOL

Multiphysics [25], which should help to address these factors. For this load range, the estimated voltage and current (~2kV, <80 A) at the antenna are well within the design limits of the moderate power vacuum feedthrough being used, as shown in Fig.11. Peak voltages in the matching network are ~2 times higher and are within the 25 kV rating of the tuning capacitors. When the plasma is seeded with a small amount of argon (~1%), the Doppler-broadened 480.6 nm Ar II ion line, measured with a McPherson spectrometer 0.1 m downstream of the ICH antenna, shows a broadening of the line profile with RF power, which is indicative of ion heating. In addition, preliminary measurements of the ion energy distribution with a retarding field energy analyzer show a broadening in the distribution at larger radii, which indicates some edge power deposition. Efforts are focused on quantifying the amount and location of power coupling and will be reported in future publications.

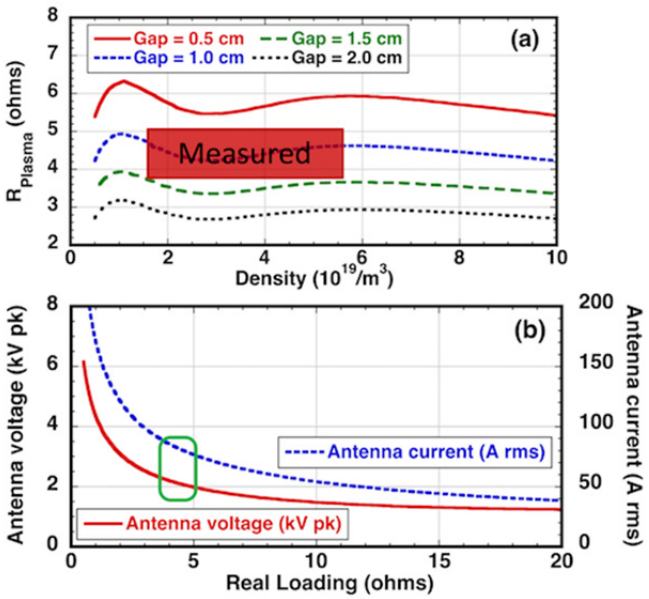

FIG. 11 (Color Online) Predicted antenna loading calculation as a function of the plasma gap using the ANTENA code (a) and the expected voltage and current on the antenna

when operated at 30 kW (a). The shaded area in (a) corresponds to the measured loading and the circle in (b) is the corresponding voltage and current for that loading range.

V. INITIAL TUNGSTEN EROSION EXPERIMENT

An initial PMI experiment exposed a sample of tungsten to a plasma of 95% helium and 5% deuterium. The purpose of the experiment was to determine whether the plasma conditions in Proto-MPEX could potentially be used for high-flux/low-fluence material tests. It has already been found that helium can lead to a change in microstructure of the material. This could affect the transport of hydrogen in tungsten [26], form nanostructure extrusions like fuzz [27], and change the thermal conductivity of tungsten [28].

For this test, a thin piece of tungsten (50 × 50 × 0.25 mm) was placed on a grounded sample holder at a location 1.5 m downstream of the helicon antenna. The plasma conditions were similar to those for the IR camera condition shown in Fig. 7b, where the magnetic field was configured such that the peak plasma heat flux was focused on a small area, with a peak magnetic field of 0.7 T. The helium gas flow was 0.05 SLM, and the central chamber pressure was ~2.5 mTorr. The sample was exposed to 55 pulses of 100 kW helicon plasmas (130 ms pulse length), with an additional 4 kW of 18 GHz power (240 ms) and 25 kW of 28 GHz power (30 ms). Based on Langmuir probe measurements, the flux is estimated to be $1–2 \times 10^{23}/m^2s$ and the fluence is estimated to be $\sim 1 \times 10^{23}/m^2$. Ion energies are estimated to be >40 eV because of the high electron temperature in this region (>20 eV).

Scanning electron microscope images from the sample, taken from the area of maximum heat flux, are shown in Fig. 12. The area evidences large grain growth and recrystallization, which typically takes place for temperatures exceeding 1400°C for tungsten. Although the temperature was not measured on this sample, it can be estimated based on the similar experimental conditions from those shown in Fig. 7b, where the temperature exceeded 300°C on a thicker (1.5 mm) 304 stainless steel target. When scaled to the thinner target and corrected with the heat capacity of tungsten, the calculated temperature exceeded 2,000°C in this area. A pitted surface can be clearly seen on the close-up view, which would be consistent with helium bubble formation. Possibly because of the low fluence of this experiment, there was no evidence of tungsten "fuzz" growth, which has been seen in other helium plasma exposure experiments. [27]

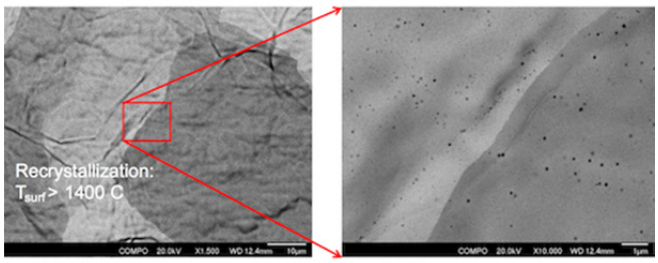

FIG. 12. Scanning electron microscopy images of a tungsten sample from the high heat flux region. Recrystallization is consistent with temperatures exceeding 1400°C. Evidence for bubble formation can be seen in the close-up view.

A transmission electron microscopy image for the sample is shown in Fig. 13. A protective layer was deposited on the surface before the sample underwent focused ion beam (FIB) milling. Bubble (cavity) formation can be seen throughout the sample,

including cavities on the order of 50 nm in diameter. Bubble location is within 100 nm of the surface.

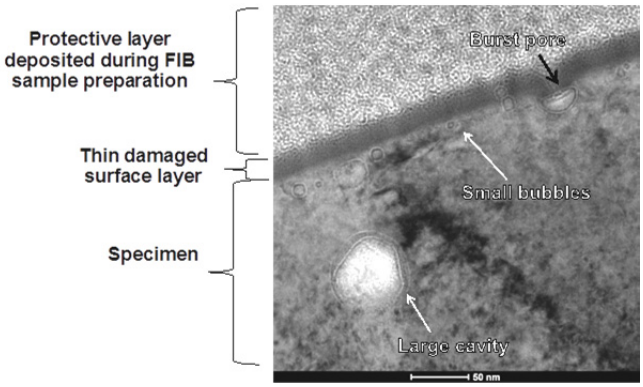

FIG. 13. Transmission electron microscopy image of a tungsten sample from the high heat flux region using a FEI F200X Talos TEM. Bubble (cavity) formation can clearly be seen, including a burst pore at the surface. The thin damage layer is likely from the FIB sample preparation.

Analysis results from the surface interface using energy-dispersive x-ray spectroscopy (EDS) are shown in Fig. 14. The elemental analysis showed no materials from the plasma chamber, such as stainless steel (from stainless steel chamber wall/skimmers) or aluminum (from the chamber wall or the helicon ceramic). Only elements from the FIB sample preparation or the TEM specimen holder were seen, assuming impurities of 0.1 to 1.0 weight % should be visible. This finding is important for future PMI experiments because any surface modifications must be attributable only to the specific plasma being used (e.g., helium or deuterium) and not from material eroded from surfaces the plasma is contacting in other parts of the chamber.

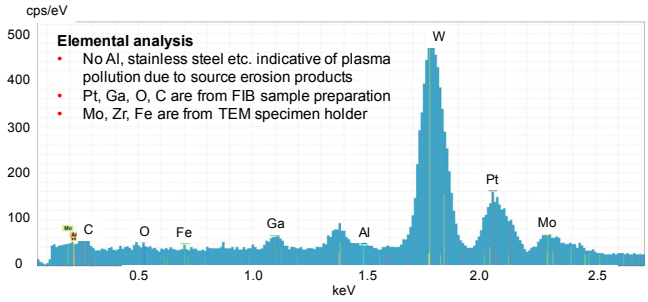

FIG. 14. EDS of the surface interface from the tungsten sample from the high heat flux region. There was no evidence of impurities from the plasma source.

SUMMARY AND CONCLUSIONS

The Proto-MPEX device has been successfully operated using deuterium and helium plasmas at peak magnetic fields of 1.5 T. In deuterium operations, the electron density and temperature near the target has reached ~$8 \times 10^{19}/m^3$ and 1.5 to 2 eV, respectively. The plasma has been observed to experience a jump from an edge-coupled mode to a center-coupled mode at sufficiently high helicon input power (>105 kW). Initial EBW experiments have shown that the electron temperature in the edge can increase up to 25% at densities above the cutoff for some experimental conditions. GENRAY-C modeling indicates that core coupling will improve at lower neutral densities, which can be achieved for longer plasma pulses and better differential pumping. The first ICH experiments have shown good antenna loading, which is consistent with modeling predictions, and quantification of ion heating is ongoing. The performance for the helicon source matches the needs of the MPEX device, and the focus of subsequent research is to demonstrate the needed electron and ion heating of the core plasma. When exposed to a high heat flux helium/deuterium plasma (~10 MW/m^2), a thin tungsten sample showed evidence of high-temperature–induced recrystallization and helium

bubble formation near the surface. No plasma source contamination was noticed on the sample surface, such as stainless steel or aluminum, which is important for the future needs of the MPEX device.

ACKNOWLEDGMENTS

The FEI F200X Talos TEM instrument was provided by the US Department of Energy, Office of Nuclear energy, Fuel Cycle R&D program, and the Nuclear Science user facilities. This material is based on work supported by the US Department of Energy, Office of Science, Office of Fusion Energy Sciences, under contract number DEAC05-00OR22725.

[1]Research Needs for Magnetic Fusion Energy Sciences - Report of the Research Needs Workshop (ReNeW), 2009, http://burningplasma.org/web/ReNeW/ReNeW.report.web2.pdf.

[2]R.A. Pitts, S. Carpentier, F. Escourbiac, T. Hirai, V. Komarov, A.S. Kukushkin, S. Lisgo, A. Loarte, M. Merola, R. Mitteau, A.R. Raffray, M. Shimada, and P.C. Stangeby, *J. Nucl. Mater*. **415**, S957 (2011).

[3]M. Rieth, J.L. Boutard, S.L. Dudarev, T. Ahlgren, S. Antusch, N. Baluc, M.-F. Barthe, C.S. Becquart, L. Ciupinski, J.B. Correia, C. Domain, J. Fikar, E. Fortuna, C.-C. Fu, E. Gaganidze, T.L. Galán, C. García-Rosales, B. Gludovatz, H. Greuner, K. Heinola, N. Holstein, N. Juslin, F. Koch, W. Krauss, K.J. Kurzydlowski, J. Linke, Ch. Linsmeier, N. Luzginova, H. Maier, M.S. Martínez, J.M. Missiaen, M. Muhammed, A. Muñoz, M. Muzyk, K. Nordlund, D. Nguyen-Manh, P. Norajitra, J. Opschoor, G. Pintsuk, R. Pippan, G. Ritz, L. Romaner, D. Rupp, R. Schäublin, J. Schlosser, I. Uytdenhouwen,

J.G. van der Laan, L. Veleva, L. Ventelon, S. Wahlberg, F. Willaime, S. Wurster, and M.A. Yar, *J. Nucl. Mater*. **417**, 463 (2013).

[4]J. Rapp, W.R. Koppers, H.J.N. van Eck, G.J. van Rooij, W.J. Goedheer, B. de Groot, R. Al, M.F. Graswinckel, M.A. van den Berg, O. Kruyt, P. Smeets, H.J. van der Meiden, W. Vijvers, J. Scholten, M. van de Pol, S. Brons, W. Melissen, T. van der Grift, R. Koch, B. Schweer, U. Samm, V. Philipps, R.A.H. Engeln, D.C. Schram, N.J. Lopes Cardozo, and A.W. Kleyn, *Fusion Eng. Des*. **85**, 1455 (2010).

[5]B. Unterberg, R. Jaspers, R. Koch, V. Massaut, J. Rapp, D. Reiter, S. Kraus, A. Kreter, V. Philipps, H. Reimer, U. Samm, L. Scheibl, B. Schweer, J. Schuurmans, I. Uytdenhouwen, R. Al, M.A. van den Berg, S. Brons, H.J.N. van Eck, W.J. Goedheer, M.F. Graswinckel, T. van der Grift, A. Kleyn, W.R. Koppers, O. Kruyt, A. Lof, H.J. van der Meiden, W. Melissen, M. van de Pol, G.J. van Rooij, P. Smeets, J. Scholten, D.C. Schram, G. De Temmerman, W. Vijvers, P.A. Zeijlmans van Emmichoven, J.J. Zielinski, *Fusion. Eng. Des*. **86**, 1797 (2011).

[6]J. Rapp, T.M. Biewer, J. Canik, J.B.O. Caughman, R.H. Goulding, D.L. Hillis, J.D. Lore, and L.W. Owen, *Fusion Sci. and Technol*. **64**, 237 (2013).

[7]J. Rapp, T.M. Biewer, T.S. Bigelow, J.B.O. Caughman, R.C. Duckworth, R.J. Ellis, D.R. Giuliano, R.H. Goulding, D.L. Hillis, R.H. Howard, T.L. Lessard, J.D. Lore, A. Lumsdaine, E.J. Martin, W.D. McGinnis, S.J. Meitner, L.W. Owen, H.B. Ray, G.C. Shaw, and V.K. Varma, *IEEE Trans. on Plasma Sci*. **44**, 3456 (2016).

[8]A. Lumsdaine, J. Rapp, V. Varma, T. Bjorholm, C. Bradley, J. Caughman, R. Duckworth, R. Goulding, V. Graves, D. Giuliano, T. Lessard, D. McGinnis, and S. Meitner, *Fusion Eng. Des*. **109-111**, 1714 (2016).

[9]S. Hiroe, R.J. Colchin, G.R. Haste, F.W. Baity, D.D. Bates, L.A. Berry, T.S. Bigelow, R.D. Burris, J.A. Cobble, W.A. Davis, R.D. Donaldson, J.C. Glowienka, D.L. Hillis, H.D.

Kimrey, R.L. Livesey, J.B. Mankin, M.W. Mcguffin, D.R. Overbey, B.G. Peterson, D.A. Rasmussen, R.K. Richards, C.R. Schaich, G.R. Sullivan, D.W. Swain, T. Uckan, T.L. White, J.B. Wilgen, R.E. Wintenberg, and K.G. Young, *Nucl. Fusion* **28**, 2249 (1988).

[10]H. Laqua, *Plasma Phys. Contr. Fusion* **49**, R1-R42 (2007).

[11]A.P. Smirnov, R.W. Harvey, and K. Kupfer, *Bull Amer. Phys. Soc*. **49**, 1626 (1994).

[12]T.H. Stix, *Waves in Plasmas* (American Institute of Physics, New York, 1992), p. 342.

[13]E.A. Bering III, F.R. Chang Díaz, J.P. Squire, T.W. Glover, M.D. Carter, G.E. McCaskill, B.W. Longmier, M.S. Brukardt, W.J. Chancery, and V.T. Jacobson, *Phys. Plasmas* **17**, 043509 (2010).

[14]B.W. Longmier, J.P. Squire, C.S. Olsen, L.D. Cassady, M.G. Ballenger, M.D. Carter, A.V. Ilin, T.W. Glover, G.E. McCaskill, F.R.C. Diaz, and E.A. Bering, *J. Propul. Power* **30**, 123 (2014).

[15]B. McVey, MIT-PFC report RR-84-12 (1984).

[16]R.J. Colchin, D.L. Hillis, R. Maingi, C.C. Klepper, and N.H. Brooks, *Rev. Sci. Instrum*. **74**, 2068 (2003).

[17]H.B. Ray, T.M. Biewer, D.T.Fehling, R.C. Isler, and E.A. Unterberg, *Rev. Sci. Instrum*. **87**, 11E711 (2016).

[18]J. Rapp, L.W. Owen, X. Bonnin, J.F. Caneses, J.M. Canik, C. Corr, J.D. Lore, *J. Nucl. Mater*. **463**, 510 (2015).

[19]T.M. Biewer, S. Meitner, J. Rapp, H. Ray, and G. Shaw, *Rev. Sci. Instrum* **87**, 11E518 (2016).

[20]M. Showers, T.M. Biewer, J.B.O. Caughman, D.C. Donovan, R.H. Goulding, and J. Rapp, *Rev. Sci. Instrum* **87**, 11D412 (2016).

[21]D. Arnuch, *Phys. Plasmas* **7**, 3042 (2000).

[22]C. MA, G. Zhao, Y. Wang, Z. Liu, L. Sang, and C. Qiang, *IEEE Trans. on Plasma Sci.* **43**, 3702 (2015).

[23]R.H. Goulding, J.B.O. Caughman, J. Rapp, T.M. Biewer, T.S. Bigelow, I.H. Campbell, J.F. Caneses, D. Donovan, N. Kafle, E.H. Martin, H.B. Ray, G.C. Shaw, M.A. Showers, *Fusion Sci. Technol.*, submitted (2016).

[24]J. Rapp, T.M. Biewer, T.S. Bigelow, J.F. Caneses, J.B.O. Caughman, R.H. Goulding, A. Lumsdaine, T. Bjorholm, C. Bradley, J.M. Canik, S.J. Diem, D. Donovan, R.C. Duckworth, R.J. Ellis, V. Graves, D. Giuliano, D.L. Green, D.L. Hillis, R.H. Howard, N. Kafle, Y. Katoh, A. Lasa, T. Lessard, E.J. Martin, S.J. Meitner, G.-N. Luo, W.D. McGinnis, L.W. Owen, H.B. Ray, G.C. Shaw, M. Showers, and V. Varma, *Nucl. Fusion*, submitted (2017).

[25]COMSOL Multiphysics v. 5.2. www.comsol.com. COMSOL AB, Stockholm, Sweden.

[26]V.Kh. Alimov, B. Tyburska-Püschel, S. Lindig, Y. Hatano, M. Balden, J. Roth K. Isobe, M. Matsuyama, and T. Yamanishial, *J. Nucl. Mater.* **370-373**, 420 (2012).

[27]M.J. Baldwin and R.P. Doerner, *Nucl. Fusion* **48**, 035001 (2008).

[28]S. Cui, M. Simmonds, W. Qin, F. Ren, G.R. Tynan, R.P. Doerner, and R. Chen., *J. Nucl. Mater.* **486**, 267 (2016).

FIG. 1 (Color Online) Cross section of the Proto-MPEX device and a typical axial magnetic field strength. The coils are labeled a M1, M2, etc. For this field calculation, there is no current in coils M2 and M5. Coils M3 and M4 have 310 amperes, and the remaining coils have 5900 amperes. The central chamber is between coils M6 and M7 and is the location of Probe A, pressure measurement P3, and the microwave launchers. The direction of the magnetic field is from left to right in the figure.

FIG. 2 (Color Online) Water-cooled helicon antenna and aluminum nitride ceramic tube.

FIG. 3 (Color Online) Waveguide extension section inside the central chamber for EBW coupling showing a +20° launch angle with respect to normal. The direction of the magnetic field is from left to right in the figure. The 8.6 cm diameter skimmer can be seen on the right.

FIG. 4 (Color Online) ICH antenna on the Proto-MPEX before insertion of the quartz tube.

FIG. 5 Backside view of the 11.4 cm diameter target plate showing an example of a fiducial pattern. Smaller fiducial patterns were used for the target patterns shown in Fig. 7. Four 1.25 cm diameter aluminum rods around the edge support the targets and keep them rigid.

FIG. 6 (Color Online) A typical plasma pulse, showing the timing of the RF and microwave systems. The 18 GHz pulse (~4 kW) starts 20 ms before the helicon pulse (~110 kW), which is referenced at t=0. The 28 GHz pulse (~25 kW) and the ICH pulse (~14 kW) are in the middle of the helicon pulse.

FIG. 7 (Color Online) Example of heat deposition profiles on the target plate. The change in the target temperature is shown (delta-T). A typical edge mode pattern (a) for a thin (d=0.25 mm) target plate. A focused-field edge mode pattern (b) for a thick (d=1.5 mm) target plate. A typical helicon-mode pattern (c) for a thin (d=0.25 mm) target plate. Units are in degrees Celsius.

FIG. 8 Plasma density (a) and temperature (b) vs. time showing the transition to a high-density mode at 35 ms, measured on-axis 1.85 m downstream of the helicon antenna. The helicon power was 110 kW, the 18 GHz power was 3 kW, the peak magnetic was 1.3 Tesla, and the magnetic field at the helicon antenna was 0.05 Tesla. The central chamber pressure was ~2 mTorr.

FIG. 9 (Color Online) Plasma density (a) and temperature (b) vs. radial position at several axial locations for the same experimental conditions shown in Fig. 8.

FIG. 10 (Color Online) Change in electron temperature and density as a function of time resulting from the injection of ~20 kW of microwave power at 28 GHz into a deuterium plasma with 110 kW of helicon power, 3 kW of 18 GHz power, and a central chamber pressure of ~2 mTorr. Data were measured 1.85 m from the helicon antenna (0.9 m from the EBW injection location) at a radius of 2 cm, with an EBW launch angle of +20°.

FIG. 11 (Color Online) Predicted antenna loading calculation as a function of the plasma gap using the ANTENA code (a) and the expected voltage and current on the antenna when operated at 30 kW (a). The shaded area in (a) corresponds to the measured loading and the circle in (b) is the corresponding voltage and current for that loading range.

FIG. 12. Scanning electron microscopy images of a tungsten sample from the high heat flux region. Recrystallization is consistent with temperatures exceeding 1400°C. Evidence for bubble formation can be seen in the close-up view.

FIG. 13. Transmission electron microscopy image of a tungsten sample from the high heat flux region using a FEI F200X Talos TEM. Bubble (cavity) formation can clearly be seen, including a burst pore at the surface. The thin damage layer is likely from the FIB sample preparation.

FIG. 14. EDS of the surface interface from the tungsten sample from the high heat flux region. There was no evidence of impurities from the plasma source.

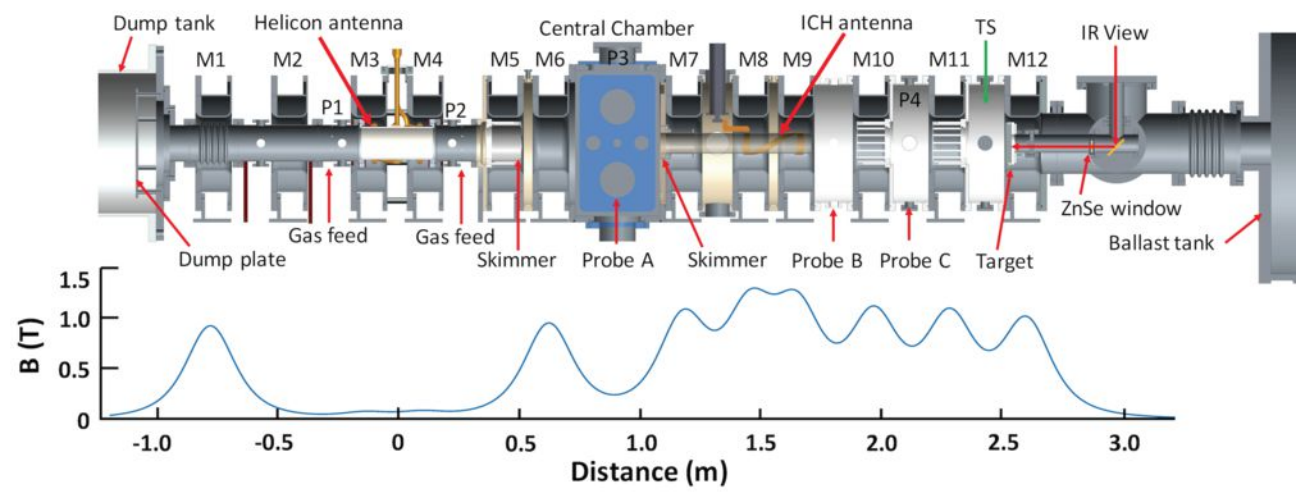
Dump tank
Helicon antenna
Central Chamber
ICH antenna
TS
IR View
M1
M2
M3
M4
M5
M6
P3
M7
M8
M9
M10
M11
M12
P1
P2
P4
Dump plate
Gas feed
Gas feed
Skimmer
Probe A
Skimmer
Probe B
Probe C
Target
ZnSe window
Ballast tank
B (T)
1.5
1.0
0.5
0
-1.0
-0.5
0
0.5
1.0
1.5
2.0
2.5
3.0
Distance (m)

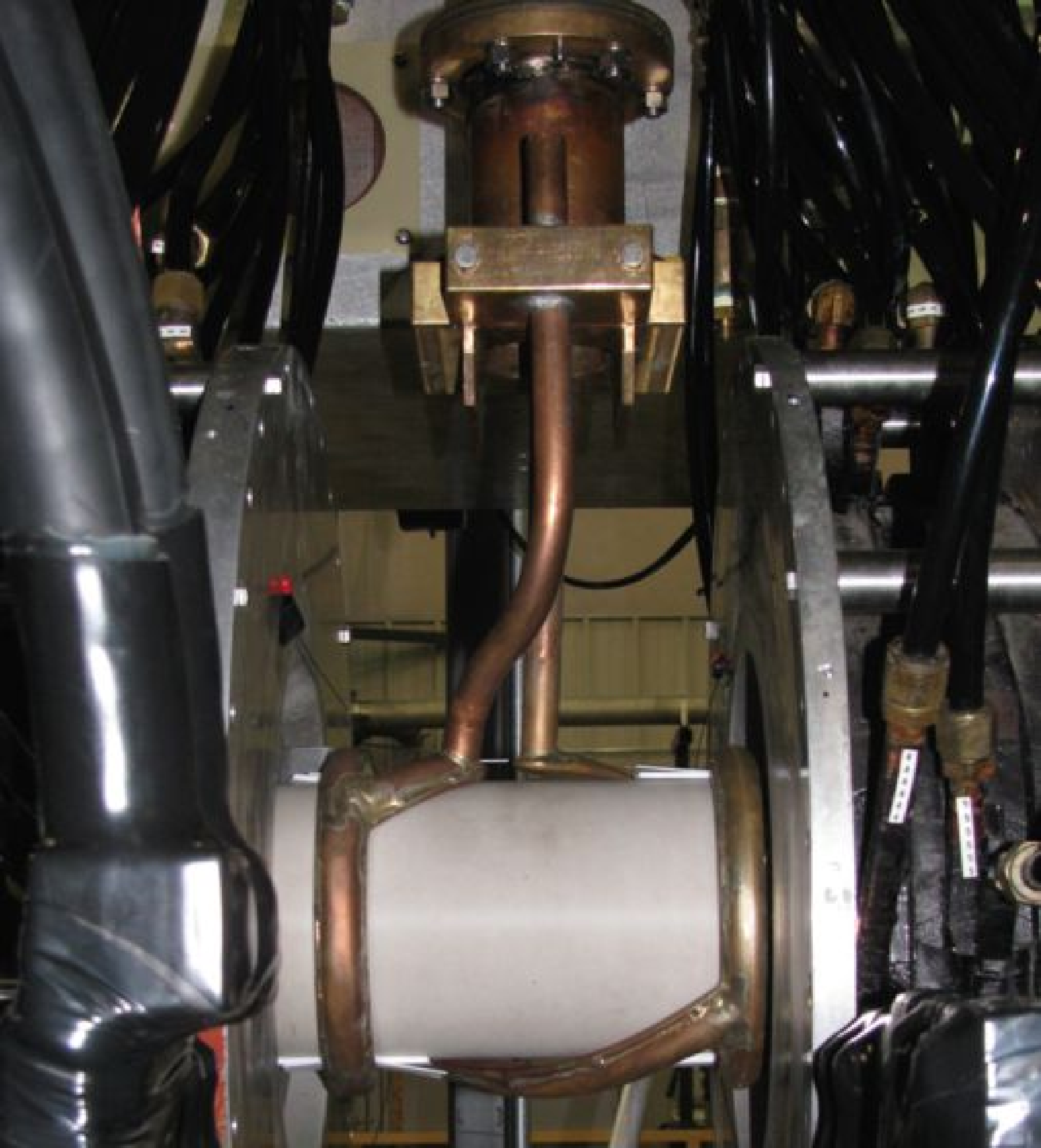

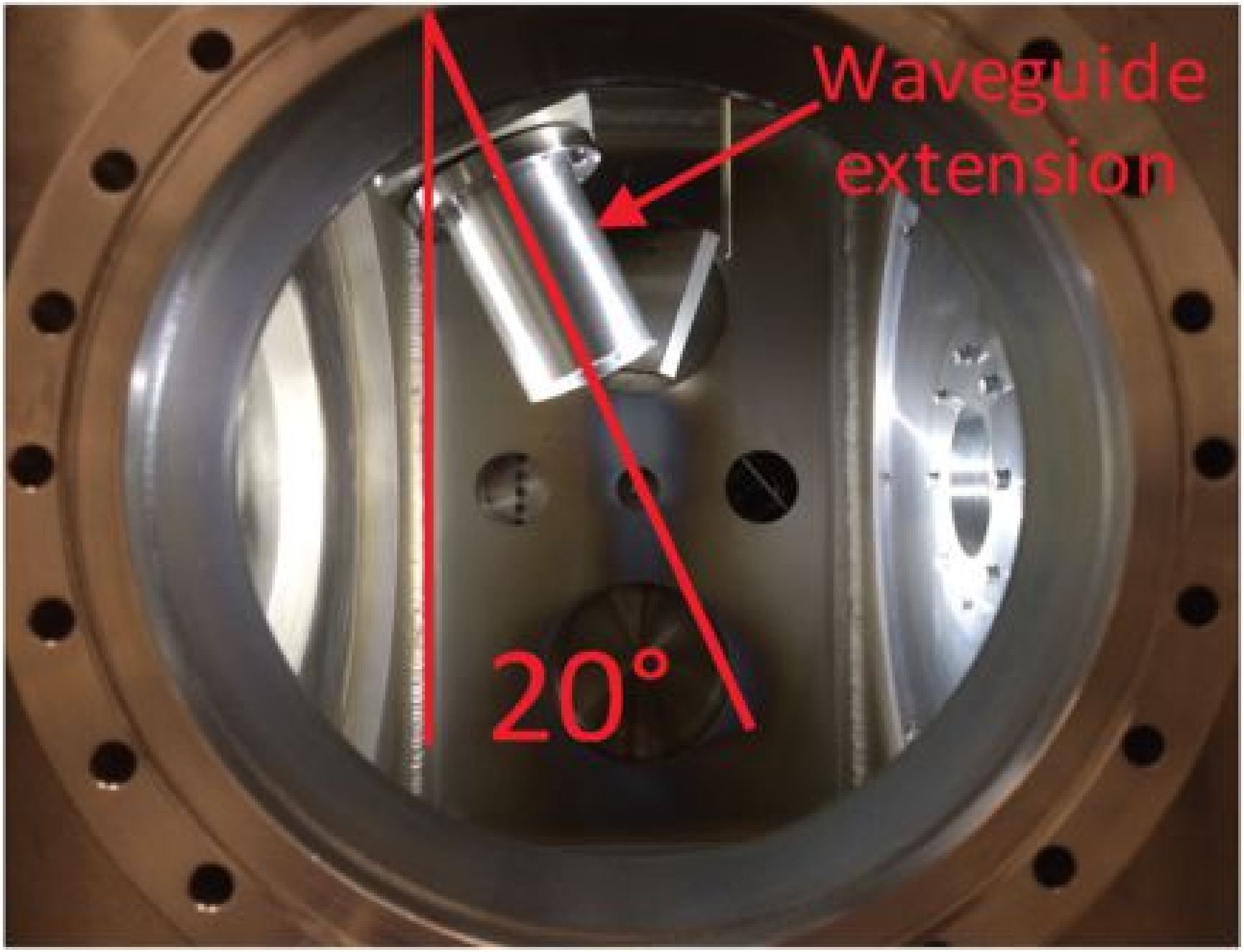
Waveguide
extension
20°

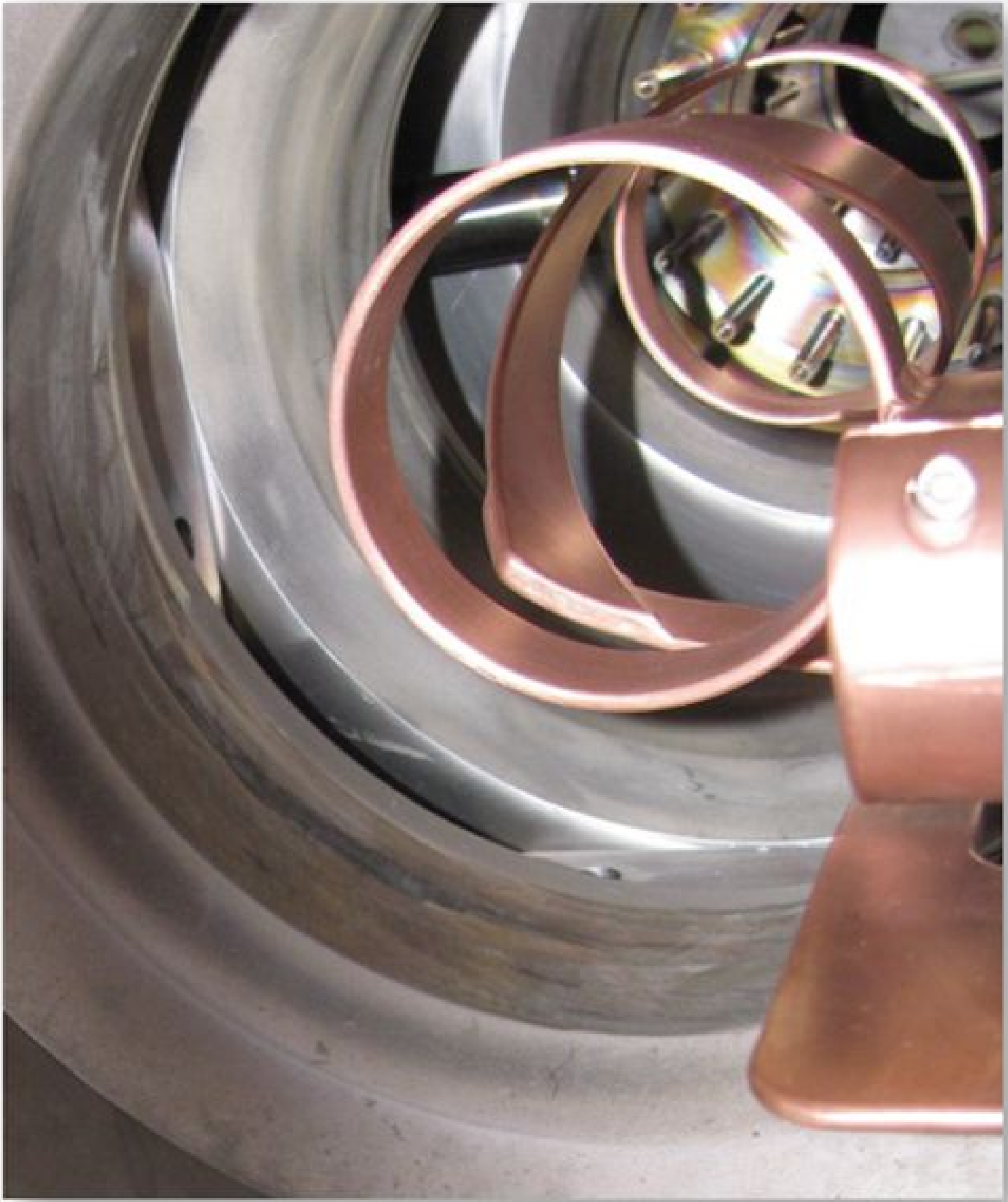

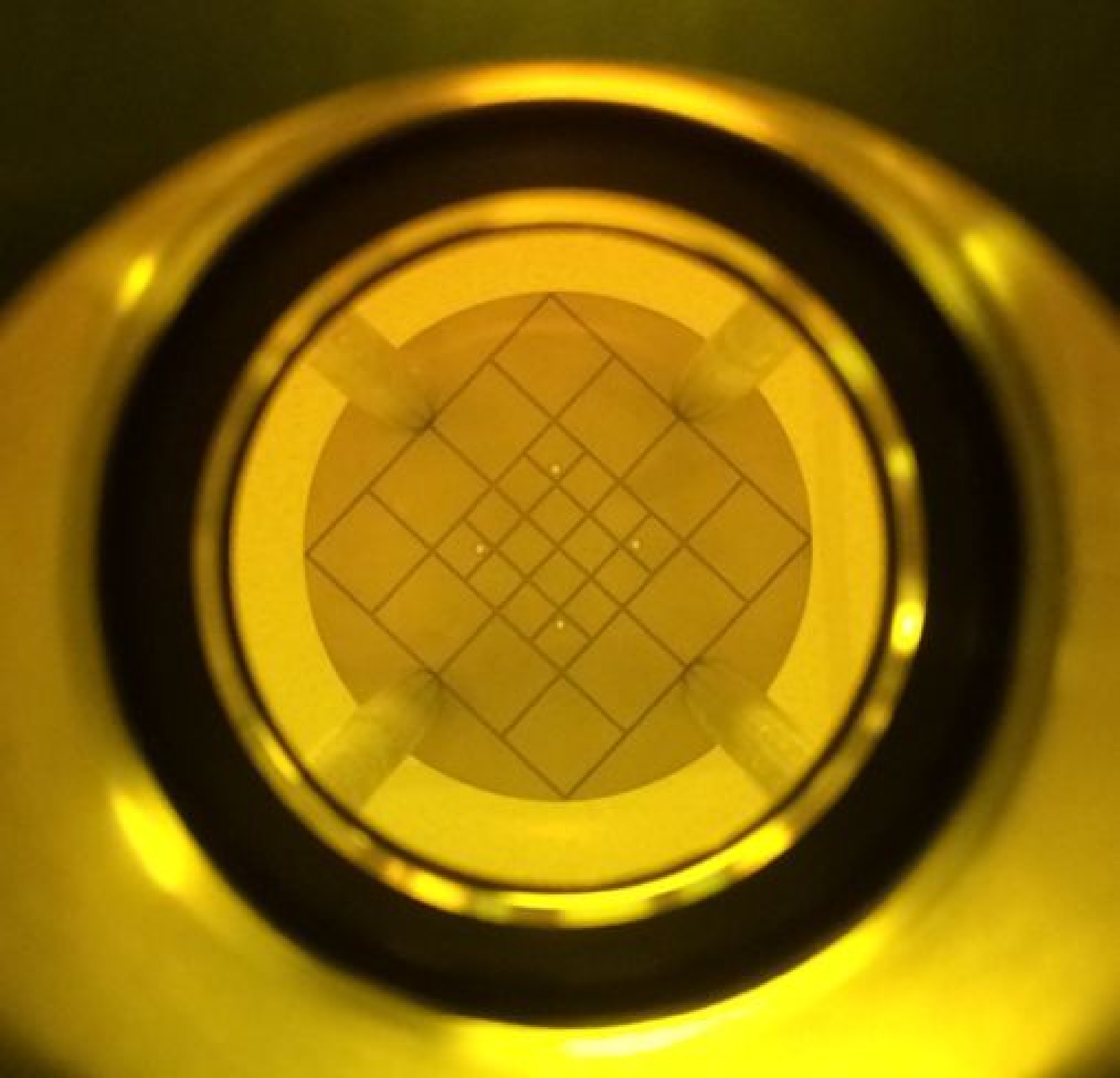

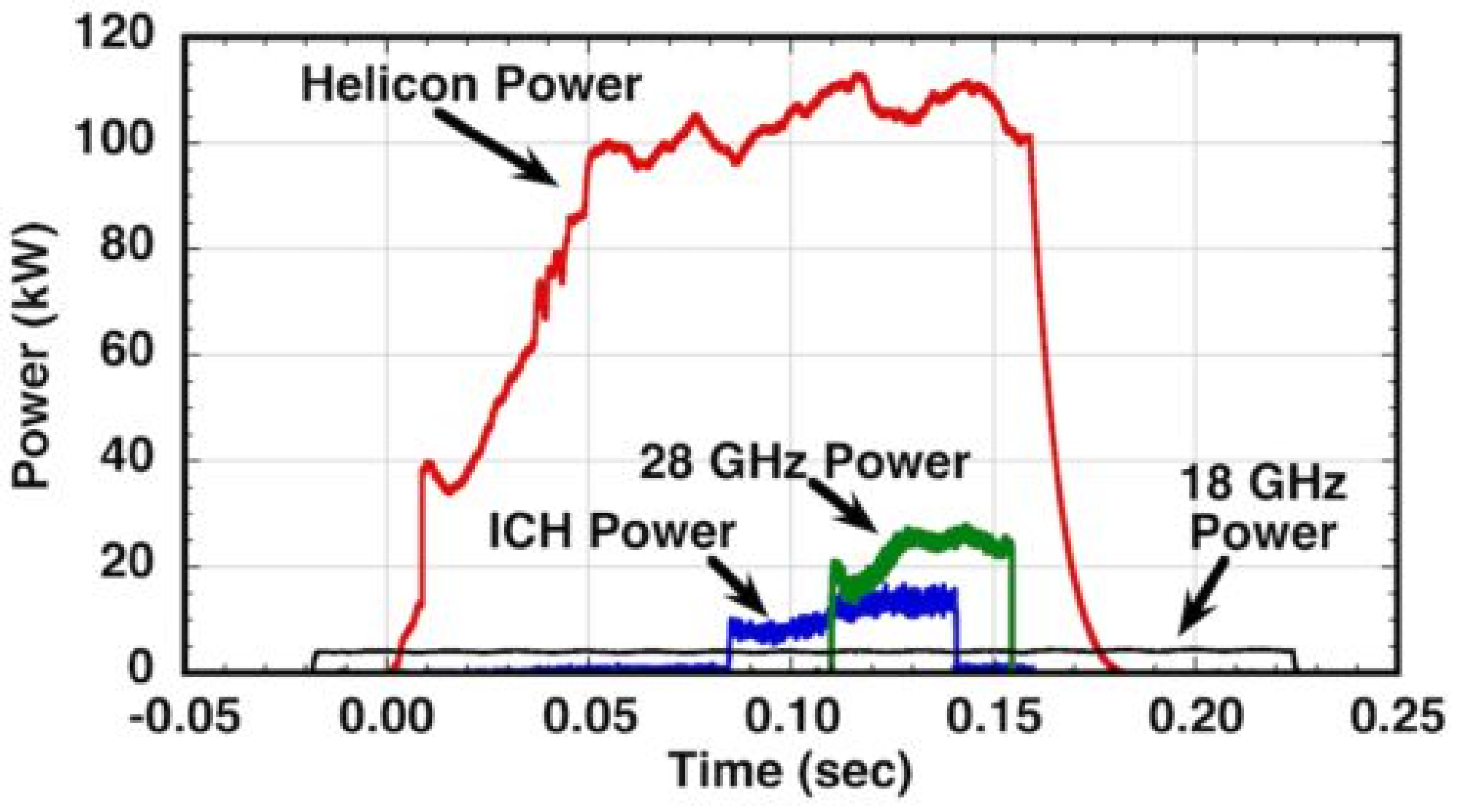
Helicon Power
28 GHz Power
ICH Power
18 GHz
Power
120
100
80
60
40
20
0
Power (kW)
-0.05
0.00
0.05
0.10
0.15
0.20
0.25
Time (sec)

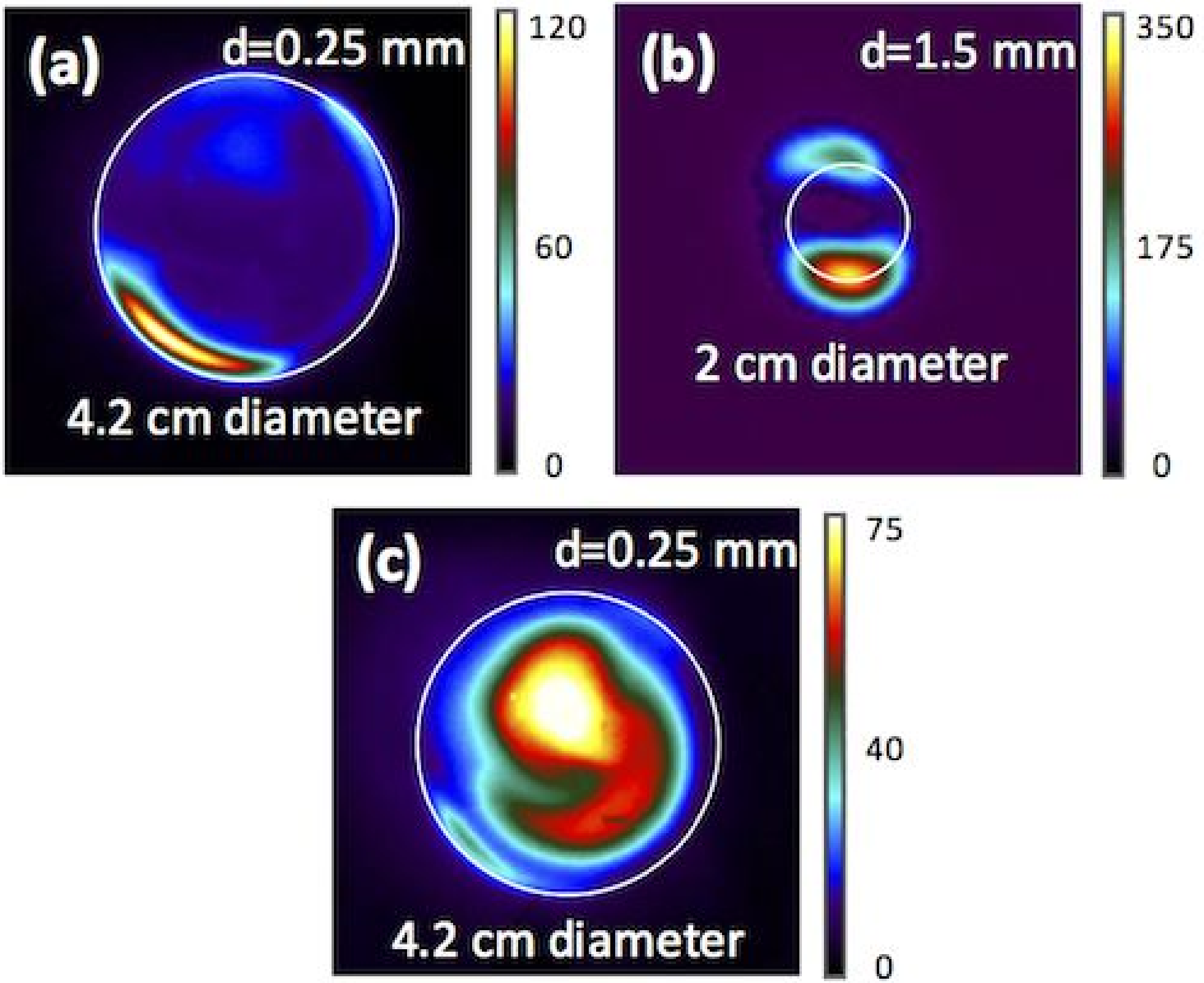
(a)
d=0.25 mm
4.2 cm diameter
120
60
0
(b)
d=1.5 mm
2 cm diameter
350
175
0
(c)
d=0.25 mm
4.2 cm diameter
75
40
0

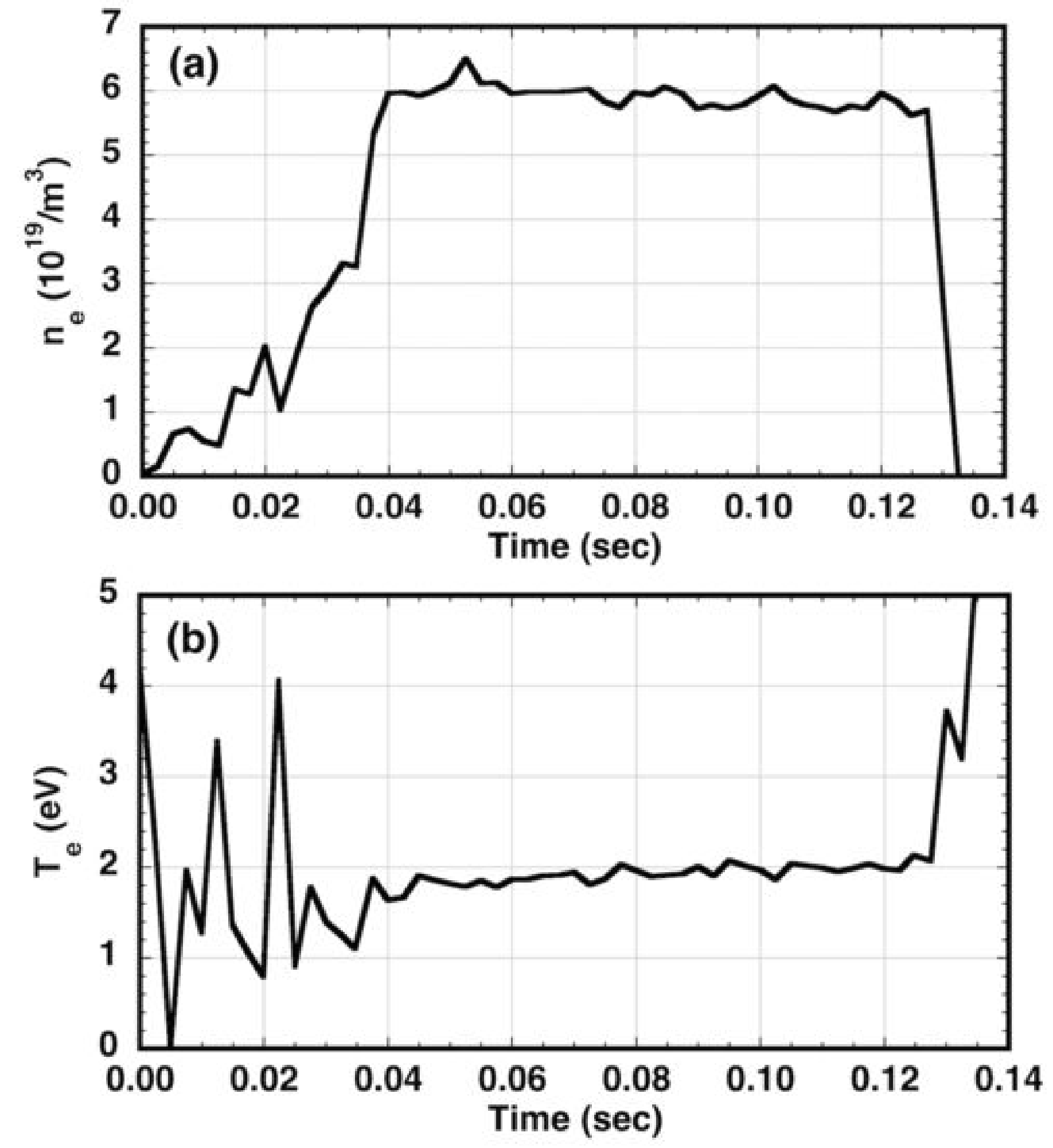
(a)
n_e (10^{19}/m^3)
0
1
2
3
4
5
6
7
0.00
0.02
0.04
0.06
0.08
0.10
0.12
0.14
Time (sec)
(b)
T_e (eV)
0
1
2
3
4
5
0.00
0.02
0.04
0.06
0.08
0.10
0.12
0.14
Time (sec)

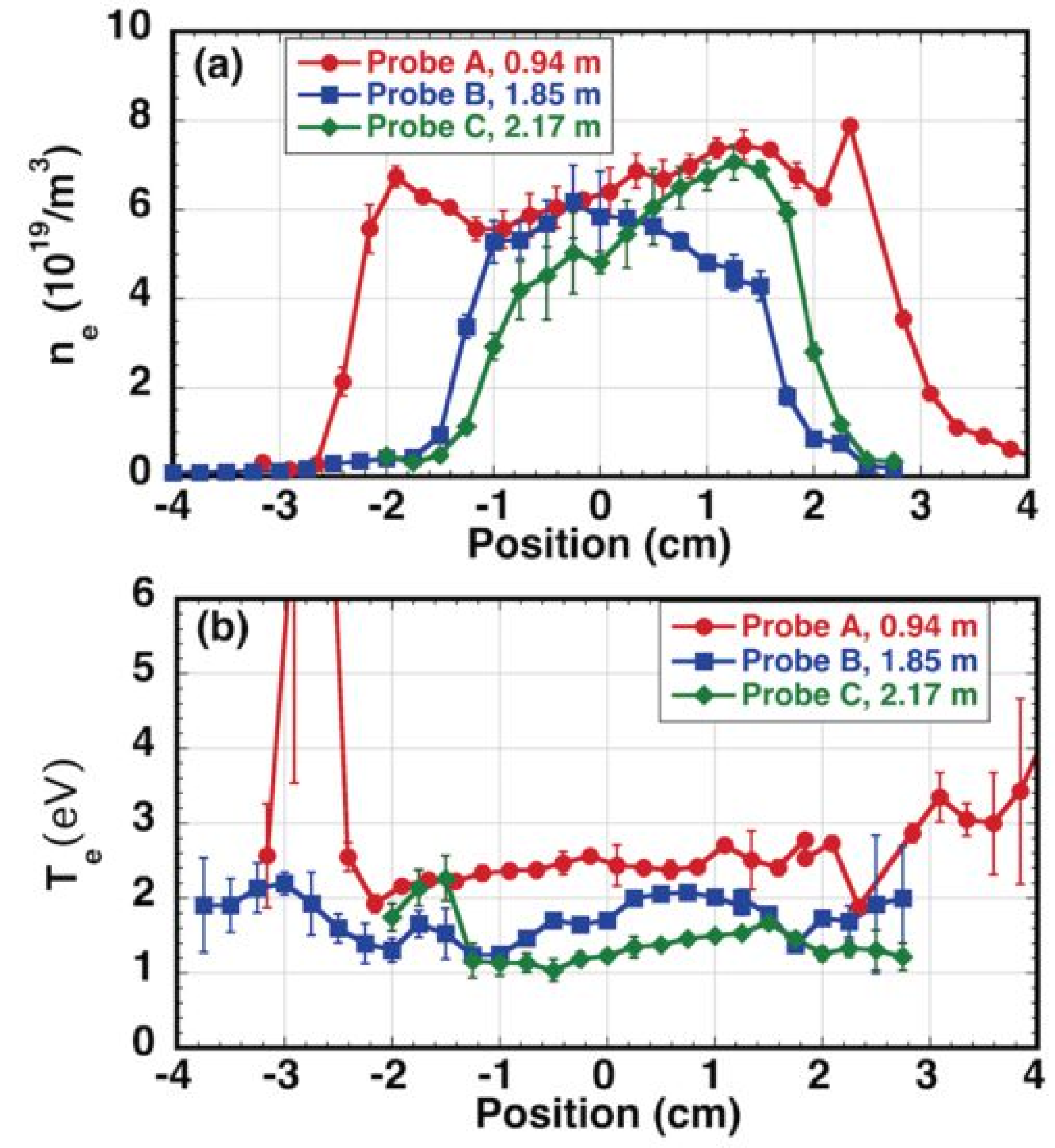
(a)
Probe A, 0.94 m
Probe B, 1.85 m
Probe C, 2.17 m
n_e (10^19/m^3)
Position (cm)
(b)
Probe A, 0.94 m
Probe B, 1.85 m
Probe C, 2.17 m
T_e (eV)
Position (cm)

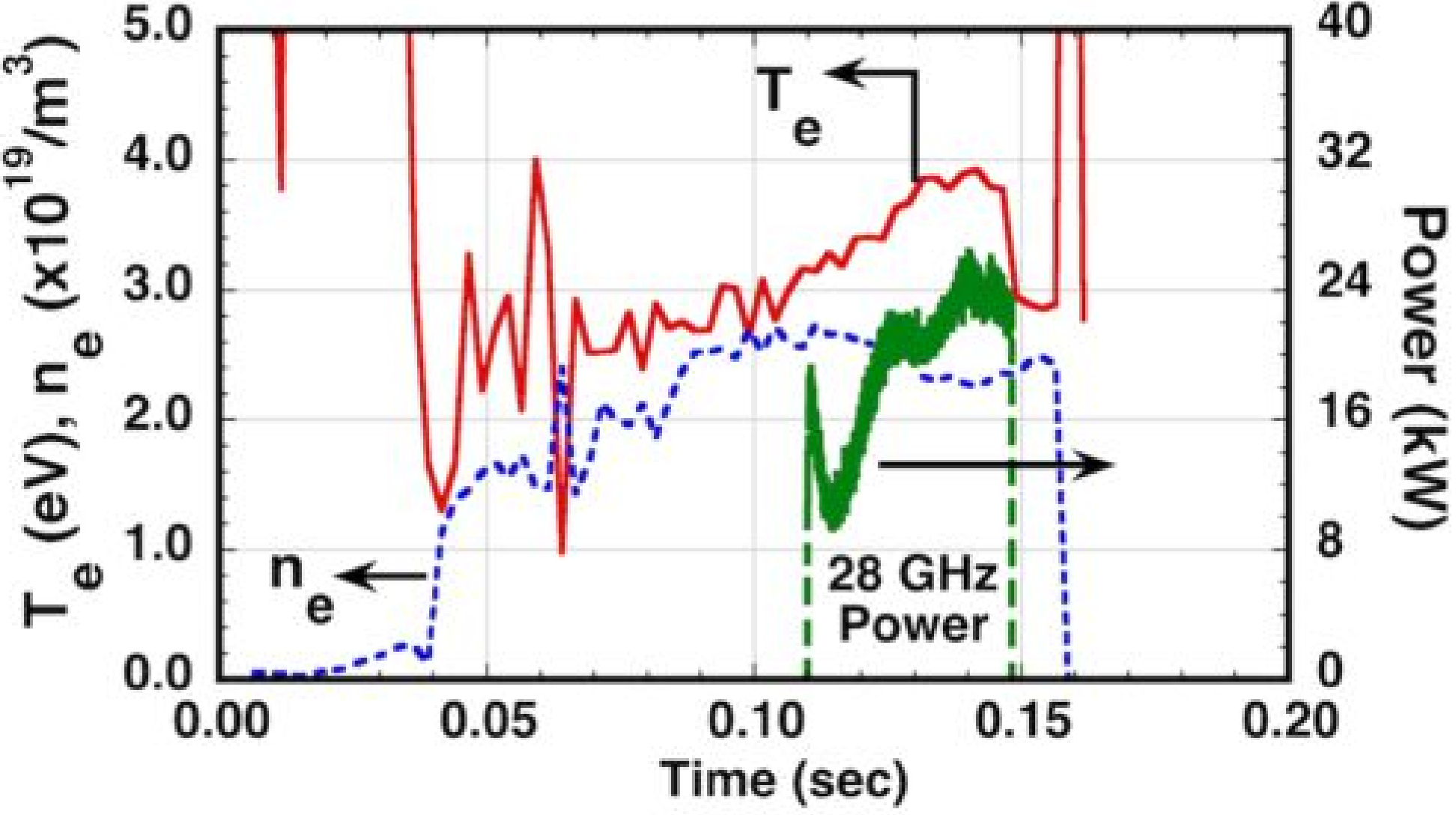
T_e (eV), n_e (x10^{19}/m^3)
Power (kW)
Time (sec)
T_e
n_e
28 GHz
Power
0.0
1.0
2.0
3.0
4.0
5.0
0
8
16
24
32
40
0.00
0.05
0.10
0.15
0.20

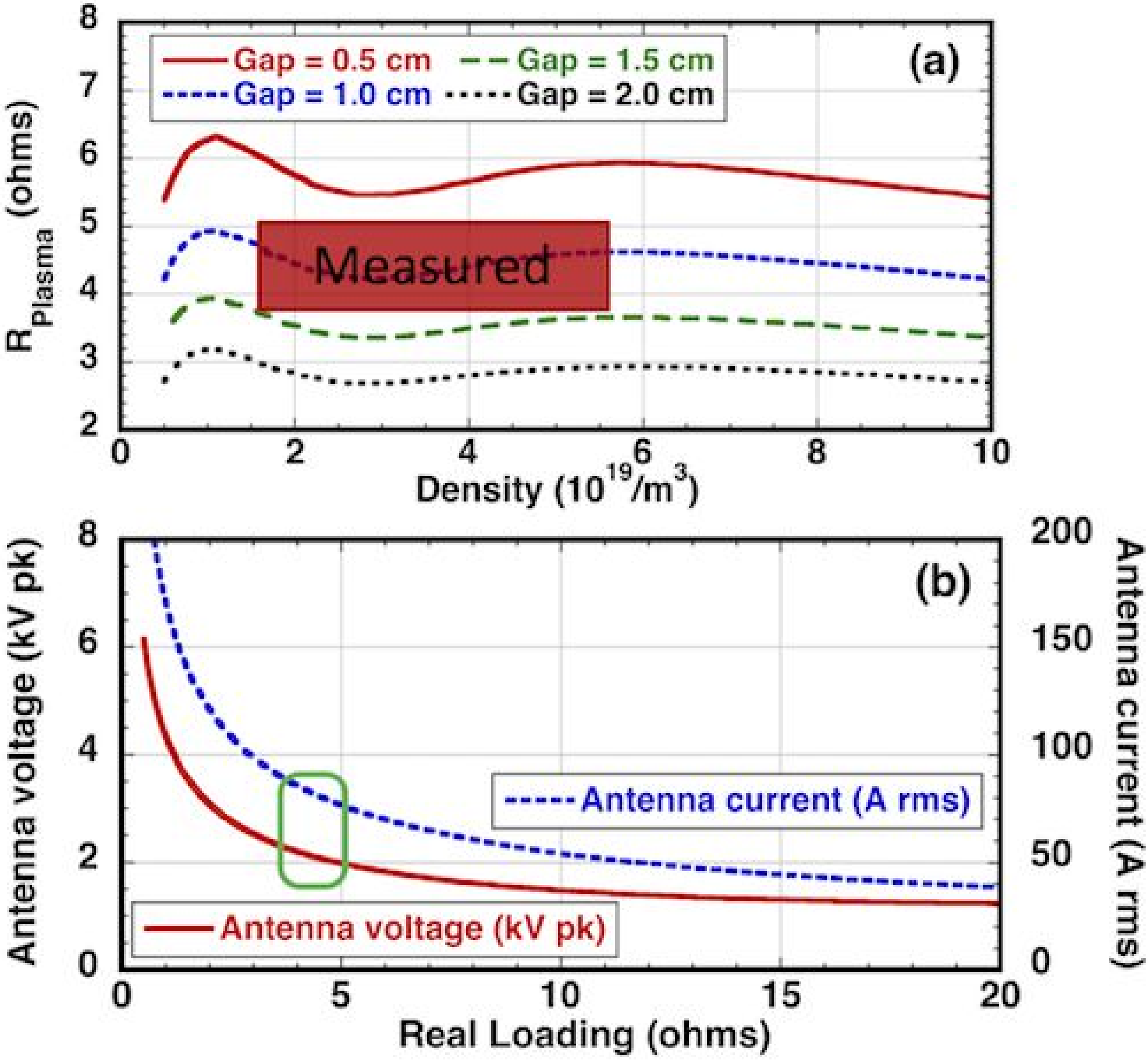
(a)
Gap = 0.5 cm
Gap = 1.5 cm
Gap = 1.0 cm
Gap = 2.0 cm
Measured
R_{Plasma} (ohms)
Density (10^{19}/m^3)
(b)
Antenna current (A rms)
Antenna voltage (kV pk)
Antenna voltage (kV pk)
Antenna current (A rms)
Real Loading (ohms)

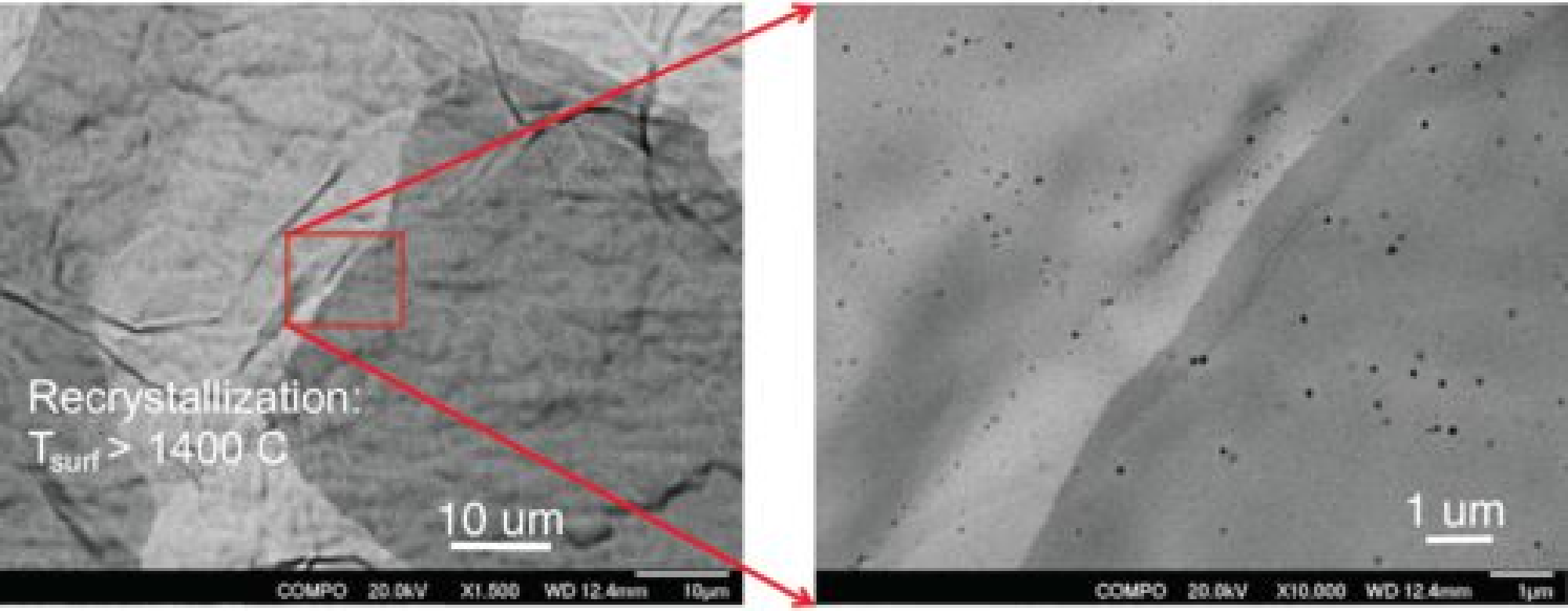
Recrystallization:
T_{surf} > 1400 C
10 um
COMPO 20.0kV X1,500 WD 12.4mm 10μm
1 um
COMPO 20.0kV X10,000 WD 12.4mm 1μm

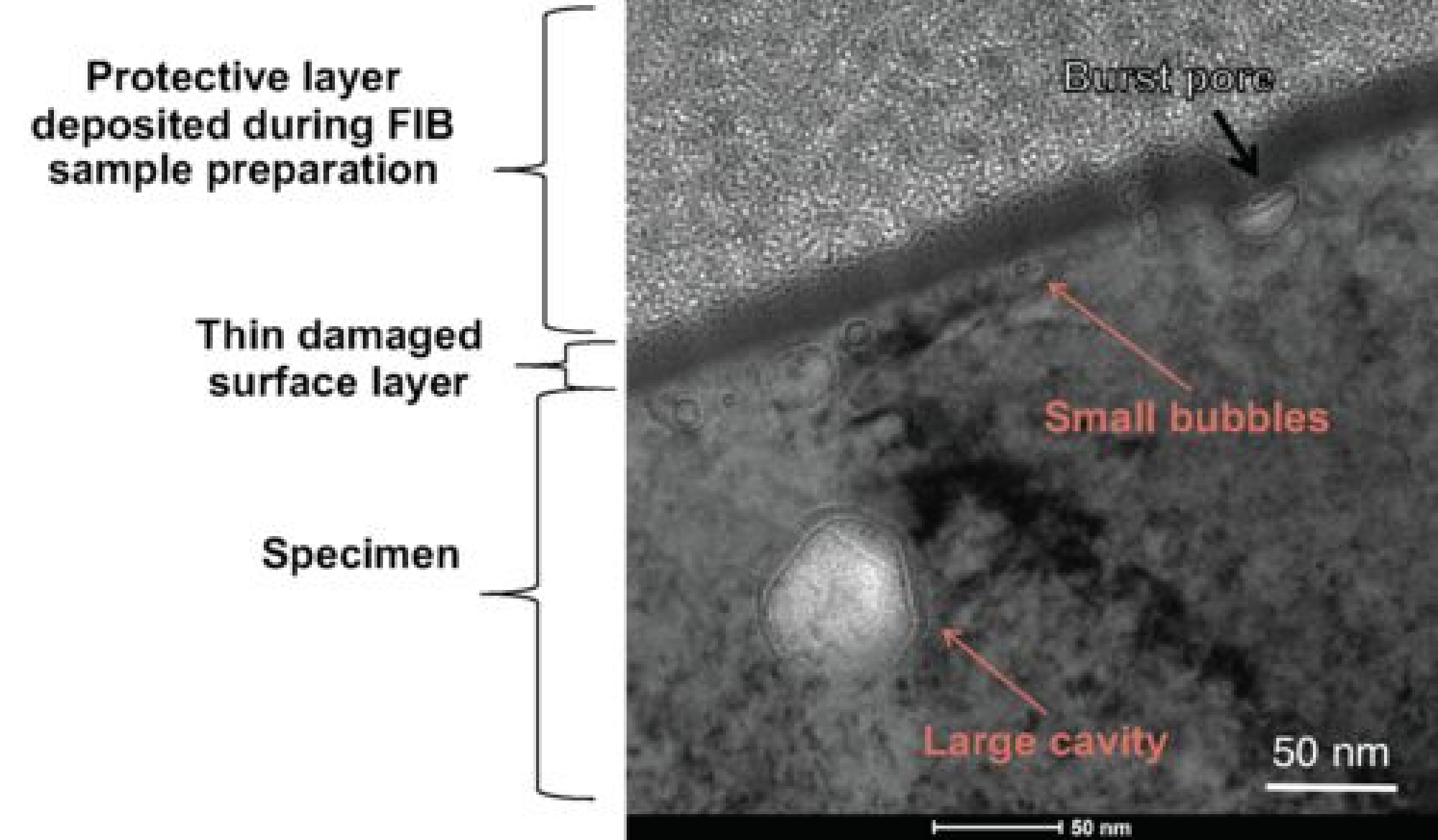
Protective layer deposited during FIB sample preparation
Thin damaged surface layer
Specimen
Burst pore
Small bubbles
Large cavity
50 nm
50 nm

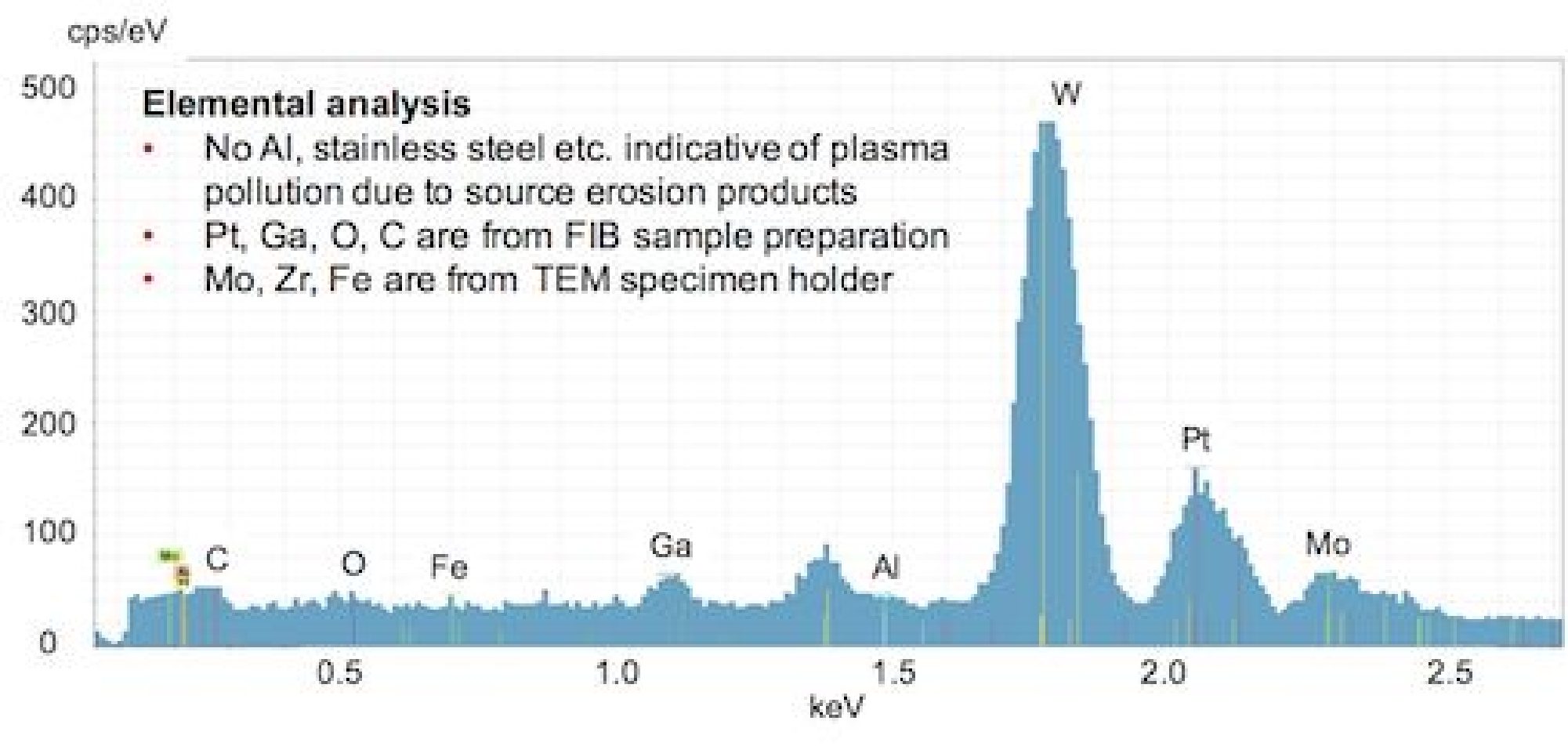
cps/eV
500
400
300
200
100
0
Elemental analysis
• No Al, stainless steel etc. indicative of plasma pollution due to source erosion products
• Pt, Ga, O, C are from FIB sample preparation
• Mo, Zr, Fe are from TEM specimen holder
W
Pt
Mo
C
O
Fe
Ga
Al
0.5
1.0
1.5
2.0
2.5
keV